






Autocorrelative weak-value amplification and simulating the protocol under strong Gaussian noiseJing-Hui Huang ^{1,2,*} Xiang-Yun Hu ^{1,†} Adetunmise C. Dada ^{3,‡} Jeff S. Lundeen,^{2,§} Kyle M. Jordan,^{2,||}
Huan Chen ⁴ and Jianqi An ⁵¹*School of Geophysics and Geomatics, China University of Geosciences, Lumo Road 388, 430074 Wuhan, China*²*Department of Physics and Centre for Research in Photonics, University of Ottawa, 25 Templeton Street, Ottawa, Ontario, Canada K1N 6N5*³*School of Physics and Astronomy, University of Glasgow, Glasgow G12 8QQ, United Kingdom*⁴*School of Mathematics and Physics, China University of Geosciences, Lumo Road 388, 430074 Wuhan, China*⁵*School of Automation, China University of Geosciences, Lumo Road 388, 430074 Wuhan, China*

(Received 11 May 2022; accepted 12 October 2022; published 3 November 2022)

By choosing more orthogonality between preselection and postselection states, one can significantly improve the sensitivity in general optical quantum metrology based on the weak-value amplification (WVA) approach. However, increasing the orthogonality decreases the probability of detecting photons and makes the weak measurement difficult, especially when the weak measurement is disturbed by strong noise and the pointer is drowned in noise with a negative-decibel signal-to-noise ratio (SNR). In this article we introduce and numerically evaluate a modified weak-measurement protocol with a temporal pointer, namely, the autocorrelative weak-value amplification (AWVA) approach. Specifically, a small longitudinal time delay (tiny phase shift) τ of a Gaussian pulse is measured by implementing two simultaneous autocorrelative weak measurements under Gaussian white noise with different SNRs. The small quantities τ are obtained by measuring the autocorrelation coefficient of the pulses instead of fitting the shift of the mean value of the probe in the standard WVA technique. Simulation results show that the AWVA approach outperforms the standard WVA technique in the time domain with smaller statistical errors, remarkably increasing the precision of weak measurement under a strong noise background.

DOI: [10.1103/PhysRevA.106.053704](https://doi.org/10.1103/PhysRevA.106.053704)**I. INTRODUCTION**

Higher precision in the measurement of various quantities is a persistent goal of scientific communities. It is well known that the pre- and postselection of the measured system have played a crucial role in amplifying detector signals in a weak measurement. The use of the pre- and postselection [1] originated from the work of Aharonov *et al.* They found theoretically that the measurement result of the component of a particle spin, called the weak value, can be amplified by a large number, which opened up a pathway for quantum metrology [2–8] with weak-value amplification (WVA).

Chronologically, a standard weak measurement includes an initial preparation of the measured system (preselection), weak coupling between the system and the pointer, a postselection of the system, and a projective measurement on the pointer to read out the results [9]. For now, the widely used pointers in weak measurements are shifts of mean values, such as temporal shifts [10–13], momentum shifts [14,15], frequency shifts [16,17], and even angular rotation shifts [18,19]. Even so, the WVA scheme entails an inherent dilemma: When the pre- and postselection are nearly orthogonal to achieve

higher sensitivity, the probability of a successful postselection will be reduced greatly [20,21]. To obtain an observable distribution function, the measurement must be repeated many times and the requirements on the apparatus are stringent [22]. For example, the resolution of the apparatus for detecting the minimum change in the input signal should be high enough and the intensity of the light source ought to be sufficiently strong to compensate for the low postselection probability. In addition, the use of photon-subtracted thermal states, which show a similar nature, has also attracted interest because of their applications in quantum metrology [23–25]. Surprisingly, an experiment [24] by implementing photon subtraction on the light exiting the interferometer can lead to an enhancement in both the magnitude of the signal and the signal-to-noise ratio (SNR).

Meanwhile, the determination of the pointer shift would inevitably be influenced by technical noise and the surrounding environment. Numerous studies [20,21,26] have been done to investigate the advantage of WVA in the presence of noise. In particular, Knee and Gauger [21] argued that the amplified displacement offered no fundamental metrological advantage, due to the necessarily reduced probability of success. Using statistically rigorous arguments, Ferrie and Combes [20] showed that the technique of WVA does not perform better than standard statistical techniques for single-parameter estimation or signal detection. Considering the measured system cannot be completely isolated from the surrounding environment and the instability of the element itself, the determination of the pointer shift will inevitably be influenced by

*jinghuihuang@cug.edu.cn

†xyhu@cug.edu.cn

‡Adetunmise.Dada@glasgow.ac.uk

§jeff.lundeen@gmail.com

||kjordan@uottawa.ca

many sources [26]: instability of the light source’s spectrum and intensity, interference of the beam with itself, thermal noise and shot noise of the detection, and other noise sources. A natural thought is to equate these types of noise with Gaussian white noise. In addition, Gaussian white noise has been replaced by colored noise (non-Gaussian) [27–30] in a variety of areas of physics, such as quantum Brownian motion in a general environment with nonlocal dissipation and colored noise [28] and non-Gaussian noise-enhanced stability of a foraging colony system [29]. Colored noise also appears in gravitational wave interferometer, where the specific noise distribution depends on the quantum state of the gravitational field [31]. However, it has long been known that white Gaussian noises can be implemented for simulating realistic experimental scenarios not only in traditional signal processing [32–34] but also in modern quantum techniques [35–37]. Therefore, in this paper we assume that the contribution of all noise is Gaussian white noise and investigate the weak-value amplification technique under a strong Gaussian white noise background.

It is encouraging that the WVA scheme based on the imaginary weak value (in the frequency domain) has sound potential to outperform the standard measurement in the presence of technical noise [10,38–42]. Furthermore, Brunner and Simon [10] proposed that the WVA scheme using the imaginary weak-value amplification can result in three orders of magnitude higher precision than the traditional interference method. Therefore, the WVA scheme based on the imaginary weak value is currently used in the field of biosensors, such as a new chiral sensor based on weak measurement for estimation of a trace amount of chiral molecule [43], a tunable and high-sensitivity temperature-sensing method via WVA of Goos-Hänchen shifts in a graphene-coated system [44], and even an optical system based on optical rotation via weak measurement for detection of the single- and double-strand states of DNA [45]. Furthermore, there have been several optimization schemes to improve the WVA scheme based on analysis of its Fisher information [26,41,46,47].

Improving the precision of temporal pointers has been studied relatively little, especially under a strong noise background. In this paper we propose a modified weak-measurement protocol with a temporal pointer, namely, autocorrelative weak-value amplification (AWVA). It is motivated by the widely used autocorrelation technique for signal denoising in engineering [48–50], where autocorrelation is a signal processing method describing the correlation of a signal with a delayed copy of itself [49]. The AWVA technique can realize the WVA scheme under a strong noise background. In particular, the measurements with Gaussian white noises are studied at a certain SNR. By simulating these measurements in SIMULINK and MATLAB, we show that the measurement with AWVA is superior to the measurement with WVA under a strong noise background.

The paper is organized as follows. In Sec. II A we briefly review the standard WVA technique for measuring a time delay τ , which serves as the coupling strength in WVA. In Sec. II B we derive the AWVA technique for the time delay τ measurement and introduce the autocorrelative intensity Θ (units of voltage) to evaluate the weak value. In Sec. III we present both the WVA scheme and the AWVA scheme under

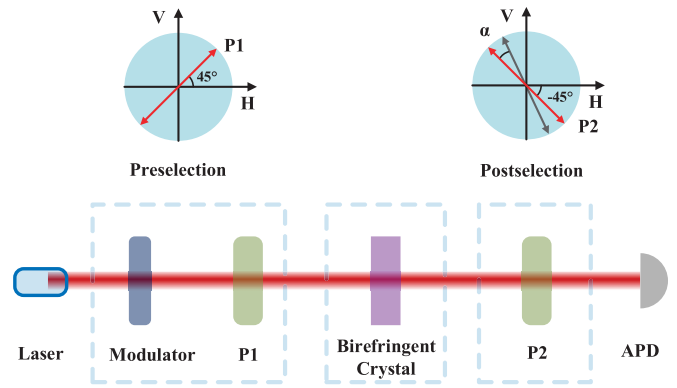


FIG. 1. Scheme of the standard WVA technique. The Gaussian beam is produced by the laser and modulator. Then photons are preselected by polarizer 1 (P1) with the optical axis set at 45° . A time delay τ (corresponding to a phase shift between the horizontal polarized state $|H\rangle$ and vertical polarized state $|V\rangle$) is induced by a birefringent crystal. Finally, the photons are postselected by the second polarizer (P2) with an optical axis set at $\alpha - 45^\circ$ and the arrival time of single photons is measured with an avalanche photodiode (APD).

Gaussian white noises. In Sec. IV we show the analytic results with various types of noises and various coupling strengths. Section V is devoted to a summary and discussion.

II. THEORY

A. Standard WVA technique

Let us briefly review the standard WVA technique of Ref. [10] with a two-level system (corresponding to the polarization state of the beam) in a quantum state $|\Phi\rangle$ and a measurement device represented by a temporal pointer $|\Psi\rangle$ to estimate a time delay. The scheme is shown in Fig. 1. First, the system is preselected in a polarized state

$$|\Phi_i\rangle = \sin\left(\frac{\pi}{4}\right) |H\rangle + \cos\left(\frac{\pi}{4}\right) |V\rangle = \frac{1}{\sqrt{2}}(|H\rangle + |V\rangle), \quad (1)$$

where $|H\rangle$ and $|V\rangle$ represent the horizontal and vertical polarized states, respectively. Thus, the initial joint state of the system and the pointer is given by

$$|\Phi_i\rangle \otimes |\Psi_i\rangle \equiv |\Phi_i\rangle |\Psi_i\rangle = \frac{1}{\sqrt{2}}(|H\rangle + |V\rangle) |\Psi_i\rangle, \quad (2)$$

where \otimes denotes tensor product. Note that the laser prepares a (bright) quantum coherent state of the field for the autocorrelation measurements. A coherent state is what a laser prepares, but other types of light would work for our scheme as well. In particular, the state must be strong or bright so that we can neglect the SNR due to the photon statistics of the particular quantum state of light in the following analysis in Sec. IV A. Then the system and the pointer are weakly coupled with the interaction Hamiltonian $\hat{H} = \tau \hat{A} \otimes \hat{p}$, where the observable operator $\hat{A} = |H\rangle \langle H| - |V\rangle \langle V|$. For a temporal pointer, \hat{q} is the longitudinal position along the central propagation direction in a frame copropagating with the light. In turn, the momentum operator \hat{p} is the frequency in the spectrum of the pointer light. In the regime of weak measurement, the time

shift τ is much smaller than the pointer spread ω , and the final state of the pointer is given by

$$\begin{aligned} |\Psi_f\rangle &= \langle\Phi_f| e^{-i\tau\hat{A}\otimes\hat{p}} |\Psi_i\rangle |\Phi_i\rangle \\ &\approx \langle\Phi_f| [1 - i\tau\hat{A}\otimes\hat{p}] |\Psi_i\rangle |\Phi_i\rangle \\ &= \langle\Phi_f|\Phi_i\rangle [1 - i\tau A_w \hat{p}] |\Psi_i\rangle \\ &= \langle\Phi_f|\Phi_i\rangle e^{-i\tau A_w \hat{p}} |\Psi_i\rangle, \end{aligned} \quad (3)$$

where $A_w := \langle\Phi_f|\hat{A}|\Phi_i\rangle/\langle\Phi_f|\Phi_i\rangle$, the so-called weak value [1], represents the mean value of observable \hat{A} . Note that the time shift τ can be amplified by the weak value A_w . Normally, the weak value A_w is a complex number [51]. In particular, the imaginary part of A_w is associated with a shift of the pointer in momentum space, while the time shift τ in the position of the pointer is amplified by the real part of A_w [52]:

$$\Delta\langle\hat{q}\rangle = \frac{\int dq q |\langle q|\Psi_f\rangle|^2}{\int dq |\langle q|\Psi_f\rangle|^2} = \tau \text{Re}(A_w). \quad (4)$$

In this paper we design the weak measurement in the time domain and prepare the initial pointer with the Gaussian profile by a modulator, where the modulator represents an acoustic optical or electro optical modulator for creating Gaussian-shaped pulses of length ω . Normally, a standard laboratory function generator and a high-voltage amplifier are required to drive the modulator. Then the initial pointer $I_1^{\text{in}}(t; \tau)$ can be obtained,

$$I_1^{\text{in}}(t; \tau) = |\langle t|\Psi_i\rangle|^2 = I_0 \frac{1}{(2\pi\omega^2)^{1/4}} e^{-(t-t_0)^2/4\omega^2}, \quad (5)$$

where I_0 represents the normalization factor. In order to amplify the ultrasmall time shift τ , the system is postselected into the state

$$|\Phi_f\rangle = \sin\left(-\frac{\pi}{4} + \alpha\right) |H\rangle + \cos\left(-\frac{\pi}{4} + \alpha\right) |V\rangle, \quad (6)$$

where $\alpha \neq 0$ in Eq. (6) to ensure the postselection probability is not zero. One then obtains the weak value as

$$A_w = \frac{\sin(-\frac{\pi}{4} + \alpha) - \cos(\frac{\pi}{4} + \alpha)}{\sin(-\frac{\pi}{4} + \alpha) + \cos(\frac{\pi}{4} + \alpha)} = -\cot\alpha. \quad (7)$$

The corresponding time shift τ can be obtained from the peak shift $\delta t = |\tau \text{Re}(A_w)| = \tau \cot\alpha$ of the signal detected by an avalanche photodiode (APD), with the detected signal I_1^{out} calculated from Eq. (3) as

$$\begin{aligned} I_1^{\text{out}}(t; \tau) &= |\langle\Phi_f|\Phi_i\rangle|^2 e^{-2i\tau A_w \hat{p}} |\langle q|\Psi_i\rangle|^2 \\ &\approx I_0 \frac{(\sin\alpha)^2}{(2\pi\omega^2)^{1/4}} e^{-(t-t_0-\delta t)^2/4\omega^2}. \end{aligned} \quad (8)$$

In principle, a larger peak shift δt and a larger weak value are obtained by choosing a smaller α , at the cost of decreasing the probability of postselection $\mathcal{P} = |\langle\Phi_f|\Phi_i\rangle|^2 = (\sin\alpha)^2$. Note that the low probability \mathcal{P} leads to a weak signal and makes the weak measurement more difficult under a strong noise background. In the next section, we will improve it with the AWVA technique.

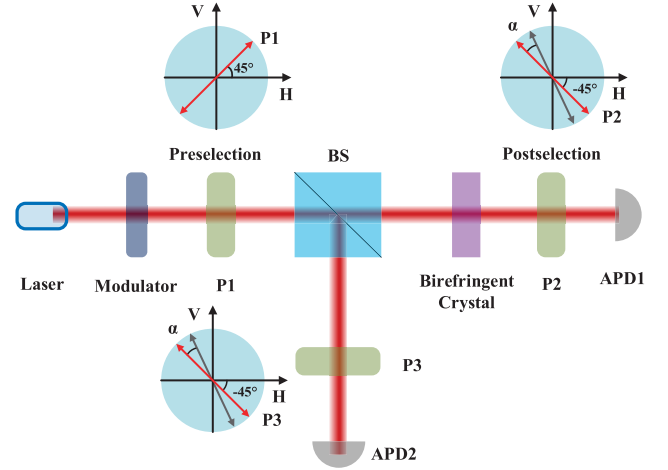


FIG. 2. Scheme of the AWVA technique. The light path is similar to that in the WVA scheme (Fig. 1), except for a 50:50 beam splitter being inserted between polarizer P1 and the birefringent crystal to add a light path for an autocorrelative measurement. The optical axis of polarizer 3 (P3) is also set at $\alpha - 45^\circ$.

B. AWVA technique with autocorrelative intensity

We display the scheme of the AWVA technique in Fig. 2, in which we introduce an autocorrelative intensity Θ for estimating the time shift τ introduced by the birefringent crystal. The main difference between the two schemes is that an additional light path is added in the AWVA scheme, by dividing the light after preselection into two light paths with a beam splitter (BS) (splitting ratio 50:50). In one path, light passes through the birefringent crystal and polarizer 2 (P2) as in the WVA scheme, while in the other path light passes only through polarizer 3 (P3) for an autocorrelative measurement. The autocorrelative measurement is prepared for obtaining the autocorrelative intensity Θ , which is defined in Eq. (11) and will be explained later in this section.

The signal $I_{21}^{\text{out}}(t)$ detected at APD1 is similar to Eq. (8) except the intensity is halved by the BS,

$$I_{21}^{\text{out}}(t; \tau) = \frac{I_0}{2} \frac{(\sin\alpha)^2}{(2\pi\omega^2)^{1/4}} e^{-(t-t_0-\delta t)^2/4\omega^2}. \quad (9)$$

Considering the light only passing through P3, there is no shift of the mean value of the pointer and the signal $I_{22}^{\text{out}}(t; \tau)$ detected at APD2 is given as

$$I_{22}^{\text{out}}(t; \tau) = \frac{I_0}{2} \frac{(\sin\alpha)^2}{(2\pi\omega^2)^{1/4}} e^{-(t-t_0)^2/4\omega^2}. \quad (10)$$

Note that there are two subscripts in $I_{21}^{\text{out}}(t; \tau)$ and $I_{22}^{\text{out}}(t; \tau)$. The first subscript 2 represents the result of the AWVA measurement. The second subscripts 1 and 2 represent the signals from APD1 and APD2, respectively. In this paper we introduce the new quantity Θ to estimate the time shift τ rather than the peak shift of the pointer. Here Θ is measured with the scheme shown in Fig. 3. The signals $I_{21}^{\text{out}}(t; \tau)$ and $I_{22}^{\text{out}}(t; \tau)$ detected at APD1 and APD2 pass through the product and the integrator. Finally, the scope detects the Θ signal, which is

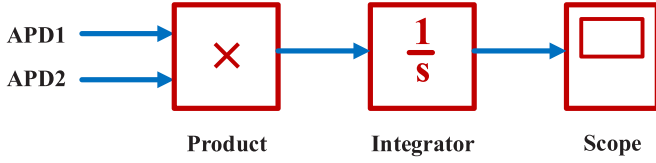


FIG. 3. Scheme of the signal processing module with the AWVA technique

mathematically given as

$$\begin{aligned} \Theta_A(t; \tau) &= \int_0^t I_{21}^{\text{out}}(t'; \tau) I_{22}^{\text{out}}(t'; \tau) dt' \\ &= \frac{I_0^2}{4} \frac{(\sin \alpha)^4}{(2\pi\omega^2)^{1/8}} \int_0^t e^{-[(t'-t_0)^2 + (t'-t_0-\delta t)^2]/4\omega^2} dt'. \end{aligned} \quad (11)$$

The numerical results in the absence of noises in the WVA scheme and the AWVA scheme are displayed in Fig. 4. In the WVA scheme, the time shift τ can be estimated by fitting the Gaussian signals $I_1^{\text{out}}(\tau = 0 \times 10^{-9} \text{ s})$ and $I_1^{\text{out}}(\tau = 3 \times 10^{-9} \text{ s})$ by means of the least-squares method. In the AWVA scheme, the time shift τ is estimated with the values of Θ . Equation (11) also indicates that the value of $\Theta_A(t; \tau)$ depends strongly on the integral time t , which affects the sensitivity of the measurement with the AWVA technique. We will show and discuss the results in the next section.

Note that the additional resources employed for the AWVA scheme in comparison to the WVA scheme include the beam splitter, polarizer 3, and correlated intensity detection, which can be implemented with product and integrator modules in Fig. 3 or coincidence detection using time-correlated single-photon counting for the measurements in the photon-starved regime. Furthermore, in the meteorological sense, the resources are the fundamental restrictions that determine the precision (e.g., the total measurement time, the total number of input photons, or the number of photons that interact with the sample or the number that are detected). Therefore, we highlight the following information for the difference between the WVA protocol and the AWVA protocol: The AWVA protocol uses twice as many input photons as the WVA protocol. However, the number of photons that interact with the crystal is the same for AWVA and WVA. Other resources (e.g., mea-

surement time) are the same for both WVA and AWVA, so they are less important to discuss.

The signal processing module shown in Fig. 3 can be implemented by both digital circuits and analog circuits. However, in this paper we will only simulate the signal processing process in SIMULINK and MATLAB (see the Appendixes). The tools in SIMULINK allow us to implement weak measurements under various types of noise; these simulation results will be shown in the following section.

III. WVA AND AWVA UNDER GAUSSIAN WHITE NOISE

It has been pointed out that technical noise [20,21,26] has a great influence on weak measurements. To simulate the WVA and AWVA schemes with the temporal pointer on SIMULINK in a realistic situation, the effects of Gaussian white noises with different SNRs on the two schemes are investigated first.

In this paper we approximate the optical noise due to the instability of the light source, interference in the light path, thermal noise and shot noise of the detection, the partition noise (vacuum noise) due to the beam splitter, and noises from other unknown sources as Gaussian noise. The characteristic of Gaussian white noise is that its power spectral density and the fast Fourier transform (FFT) result are uniformly distributed. In our work the Gaussian normal distribution denoted by $\mathbf{N}(t, \sigma^2, \xi)$ is generated by the pseudorandom number generator in SIMULINK, where σ^2 is the variance of the random signal and ξ is the random seed and represents the initial value used to generate a pseudorandom number in SIMULINK. The noise $\mathbf{N}(t, \sigma^2, \xi)$ with different ξ corresponds to the results of multiple measurements (different times). Note that thermal noise and shot noise of the detection may cause the different series of noises detected on APD1 and APD2. In addition, the influence of the noise of different time series is also investigated in Sec. IV F.

The Gaussian white noise $\mathbf{N}(t, \sigma^2 = 1.0 \times 10^{-5}, \xi = 0)$, the power spectral density $\mathbf{PSD}(f, \sigma^2 = 1.0 \times 10^{-5}, \xi = 0)$, and the corresponding $\mathbf{FFT}(f, \sigma^2 = 1.0 \times 10^{-5}, \xi = 0)$ results are shown in Fig. 5. Note that Gaussian white noise is not only uncorrelated but also statistically independent between random variables at two different moments. Thus, on the basis of the autocorrelation technique for signal denoising

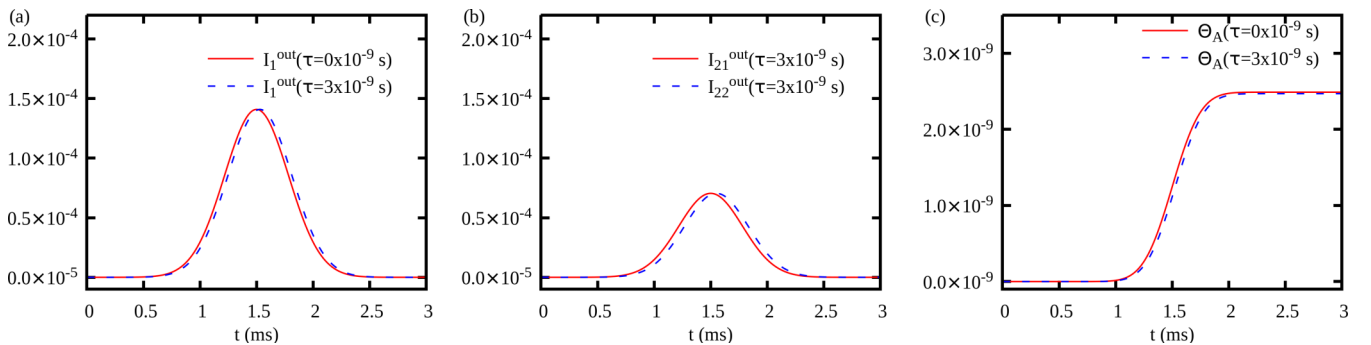


FIG. 4. Simulation results with WVA and AWVA schemes in the absence of noise: (a) signals $I_1^{\text{out}}(t; \tau)$ with $\tau = 0 \times 10^{-9} \text{ s}$ and $\tau = 3 \times 10^{-9} \text{ s}$ in the WVA scheme, (b) signals $I_{21}^{\text{out}}(t; \tau)$ as well as $I_{22}^{\text{out}}(t; \tau)$ with $\tau = 3 \times 10^{-9} \text{ s}$ in the AWVA scheme, and (c) signals I_A^{AC} with $\tau = 0 \times 10^{-9} \text{ s}$ and $\tau = 3 \times 10^{-9} \text{ s}$ in the AWVA scheme. The quantities $I_{21}^{\text{out}}(t; \tau)$, $I_{22}^{\text{out}}(t; \tau)$, and $I_{22}^{\text{out}}(t; \tau)$ are in units of I_0 and the quantity I_A^{AC} is in units of voltage.

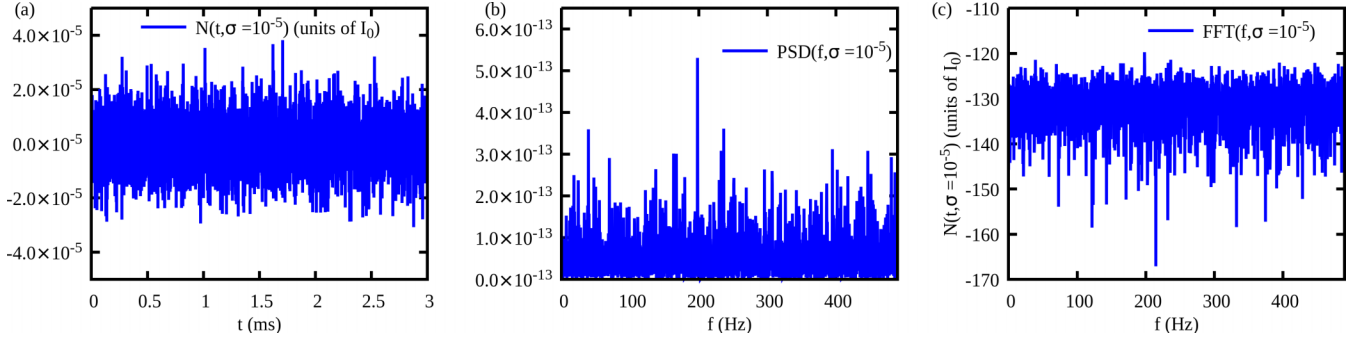


FIG. 5. (a) Gaussian noise signals $\mathbf{N}(t, \sigma^2 = 1.0 \times 10^{-5}, \xi = 0)$ in the time domain, (b) its power spectral densities $\mathbf{PSD}(f, \sigma^2 = 1.0 \times 10^{-5}, \xi = 0)$, and (c) its FFT result $\mathbf{FFT}(f, \sigma^2 = 1.0 \times 10^{-5}, \xi = 0)$.

in engineering [48–50], the $\Theta_{\text{NN}}(t; \tau)$ of the Gaussian white noise $\mathbf{N}(t, \sigma^2)$ is defined as

$$\begin{aligned} \Theta_{\text{NN}}(t; \tau) &= \int_0^t \mathbf{N}(t', \sigma^2, \xi_1) \mathbf{N}(t', \sigma^2, \xi_2) dt' \\ &= 0(t \rightarrow \infty), \end{aligned} \quad (12)$$

where ξ_1 and ξ_2 represent the different random seeds of the Gaussian white noise $\mathbf{N}(t, \sigma^2, \xi)$. In this paper, for the measurements with the AWVA technique, the corresponding time series of noises $\mathbf{N}(t, \sigma^2, \xi_1)$ and $\mathbf{N}(t, \sigma^2, \xi_2)$ detected at APD1 and APD2, respectively, ought to be different. Even if the two noises only originate from the laser (before the BS), the noise $\mathbf{N}(t, \sigma^2, \xi_1)$ which passes through the birefringent crystal and the different lengths of the two optical paths in Fig. 2 will cause a time delay between the noises $\mathbf{N}(t, \sigma^2, \xi_1)$ and $\mathbf{N}(t, \sigma^2, \xi_2)$.

Then we add the noise $\mathbf{N}(t, \sigma^2; \xi)$ to both the WVA scheme and the AWVA scheme. For the measurement with the WVA technique, we get the final signal $I_{1+\text{N}}^{\text{out}}(t; \tau)$ under $\mathbf{N}(t, \sigma^2, \xi)$ as

$$I_{1+\text{N}}^{\text{out}}(t; \tau) = I_1^{\text{out}}(t; \tau) + \mathbf{N}(t, \sigma^2, \xi). \quad (13)$$

Now we need to evaluate the mean shift δt by the Gaussian fitting the result of $I_{1+\text{N}}^{\text{out}}(t; \tau)$. Obviously, the noise $\mathbf{N}(t, \sigma^2, \xi)$ will lead to an uncertainty of estimating δt . The simulation results with different simulation conditions are shown in Fig. 6 and Tables II and IV.

For the measurement with the AWVA technique, we obtain the quantity $\Theta_{A+\text{N}}(\tau)$ with the noises $\mathbf{N}(t, \sigma^2, \xi_1)$ and $\mathbf{N}(t, \sigma^2, \xi_2)$. Then $\Theta_{A+\text{N}}(\tau)$ is defined as

$$\begin{aligned} \Theta_{A+\text{N}}(t; \tau) &= \int_0^t I_{21+\text{N}}^{\text{out}}(t'; \tau) I_{22+\text{N}}^{\text{out}}(t'; \tau) dt' \\ &= \Theta_A(t; \tau) + \Theta_{21\text{N}}(t; \tau) \\ &\quad + \Theta_{22\text{N}}(t; \tau) + \Theta_{\text{NN}}(t; \tau), \end{aligned} \quad (14)$$

with

$$\Theta_{21\text{N}}(t; \tau) = \int_0^t I_{21}^{\text{out}}(t'; \tau) \mathbf{N}(t', \sigma^2, \xi_1) dt', \quad (15)$$

$$\Theta_{22\text{N}}(t; \tau) = \int_0^t I_{22}^{\text{out}}(t'; \tau) \mathbf{N}(t', \sigma^2, \xi_2) dt'. \quad (16)$$

However, due to the noncorrelation between the signal and the random noise, we obtain that $\Theta_{21\text{N}}(t; \tau) = \Theta_{22\text{N}}(t; \tau) = 0$.

Finally, we can get the relation $\Theta_{A+\text{N}}(t; \tau) = \Theta_A(t; \tau)$ from the theoretical analysis when the integral time t is infinite, which means that the noise has no influence on evaluating the values of Θ by assuming that the noises $\mathbf{N}(t, \sigma^2, \xi_1)$ and $\mathbf{N}(t, \sigma^2, \xi_2)$ detected at APD1 and APD2, respectively, are strictly time independent. In particular, we first investigate the accuracy of the formula (12) using simulations on SIMULINK, based on Eq. (14).

Figure 7(a) shows the autocorrelative intensity $\Theta_{\text{NN}}(t; \tau)$ of various noises with different seeds ξ_1 and ξ_2 at $\text{SNR}^* = -18.6$ dB and $1/T = 1$ MHz. The values of $\Theta_{\text{NN}}(t; \tau)$ with different initial time (seed) are on the order of 2.0×10^{-11} , which is smaller than the theoretical maximum value of $\Theta_A(t; \tau)$ calculated from Eq. (11) in Fig. 4. However, with the SNR of the Gaussian noise decreasing as shown in Fig. 7(b), the values of $\Theta_{\text{NN}}(t; \tau)$ increase. The larger values may have more negative effects on the AWVA technique. We will investigate the total autocorrelative intensity $\Theta_{A+\text{N}}(t; \tau)$ in the next section. Note that “infinite” is a relative concept: When the number of integral nodes (sample time) $M \gg 1$ in the integral time t , the integral time can also be regarded as infinite. Therefore, the autocorrelative results of noises $\mathbf{N}(t, \sigma^2, \xi_1 = 0)$ and $\mathbf{N}(t, \sigma^2, \xi_2 = 700)$ at $\text{SNR}^* = -18.6$ dB with different sampling frequency $1/T$ (T corresponding to sampling interval) are displayed in Fig. 7(c). The curves indicate that increasing the sampling rate $1/T$ of the APD can decrease the value of $\Theta_{\text{NN}}(t; \tau)$ and improve the accuracy of the formula (12).

In conclusion, the equality $\Theta_{A+\text{N}}(\tau) = \Theta_A(\tau)$ represents that the AWVA scheme has strong robustness¹ against noise. The features of the realistic kinds of noise are indeed more complicated than the features of the Gaussian noise [27–30]. However, it is necessary to first consider the effects of the strong Gaussian noise on the weak measurements theoretically; the simulation results are shown in the next section.

IV. NUMERICAL RESULTS

After adding the Gaussian white noise with different SNRs to the signals, we fit the peak shift δt in the WVA scheme

¹The “robustness” of the control system refers to the ability of the system to keep a certain performance invariable under the disturbance (noise) of uncertainty.

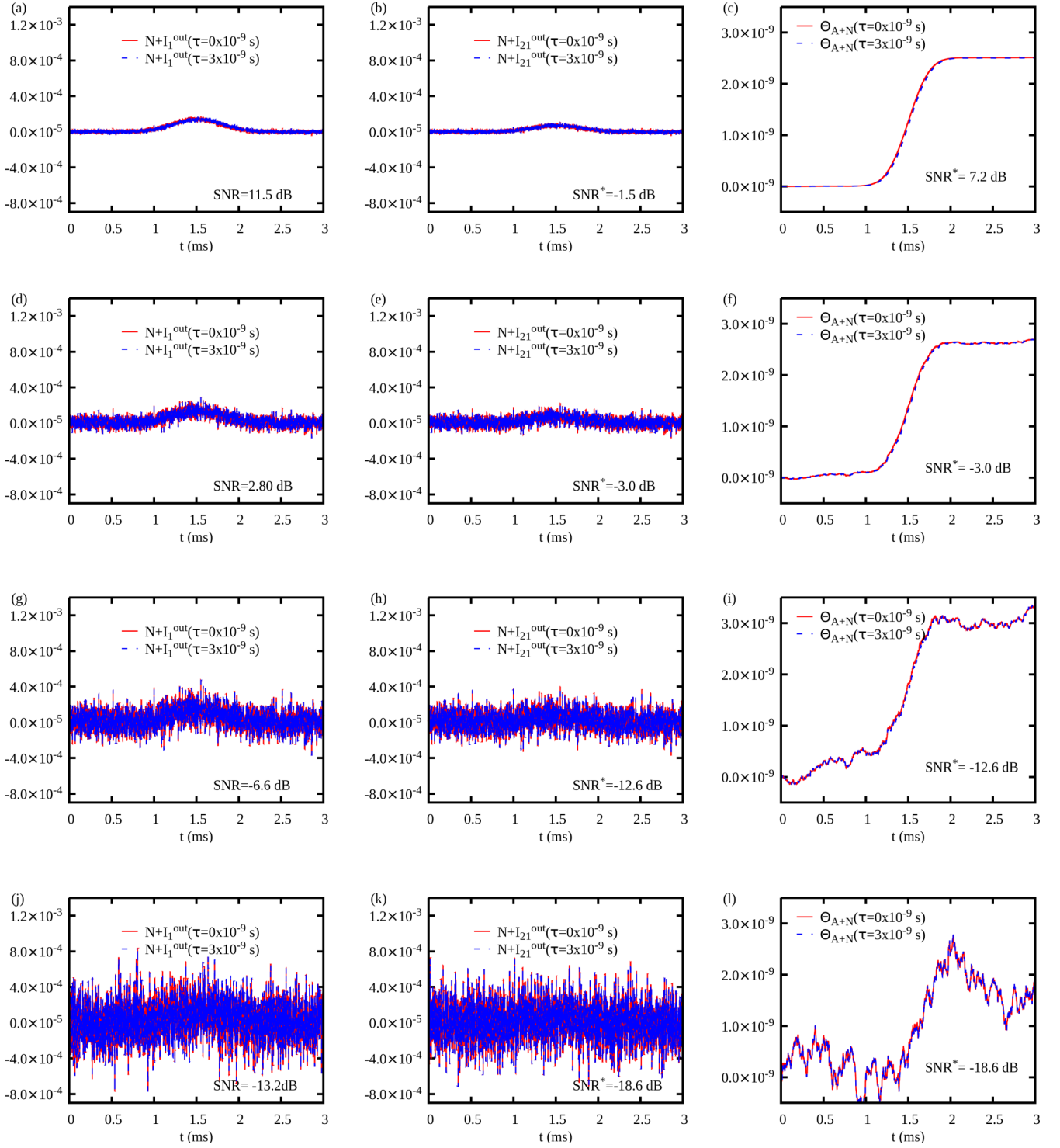


FIG. 6. Simulation results in two schemes under the Gaussian white noise with different SNR: (a), (d), (g), and (j) signals $I_1^{\text{out}}(t; \tau)$ in the WVA scheme under noise $\mathbf{N}(t, \sigma^2, \xi = 0)$; (b), (e), (h), and (k) signals $I_{21}^{\text{out}}(t; \tau)$ and $I_{22}^{\text{out}}(t; \tau)$ in the AWVA scheme; and (c), (f), (i), and (l) autocorrelative intensity Θ in the AWVA scheme under noises $\mathbf{N}(t, \sigma^2, \xi_1 = 0)$ and $\mathbf{N}(t, \sigma^2, \xi_2 = 700)$ with sampling frequency $1/T = 1$ MHz. The quantities $I_{21}^{\text{out}}(t; \tau)$, $I_{21}^{\text{out}}(t; \tau)$, and $I_{22}^{\text{out}}(t; \tau)$ are in units of I_0 and the quantity I_A^{AC} is in units of voltage.

and compute the values of Θ in the AWVA scheme. In our simulation, the initial temporal probe is chosen as

$$I_1^{\text{in}}(t; \tau) = |\langle q | \Psi_i \rangle|^2 = \frac{1}{(2\pi \times 0.0002^2)^{1/4}} e^{-(t-0.0015)^2/0.0004^2}, \quad (17)$$

where I_0 is set as unity and the angle for postselection is set as $\alpha = 0.01$ rad. Note that the sampling frequency $1/T$ of APDs has a great impact on the autocorrelative intensity Θ_{NN} in the AWVA scheme, which was discussed in the preceding section. Therefore, the simulation of the final autocorrelative intensity Θ_{A+N} with $1/T = 1, 10,$ and 100 MHz is investigated.

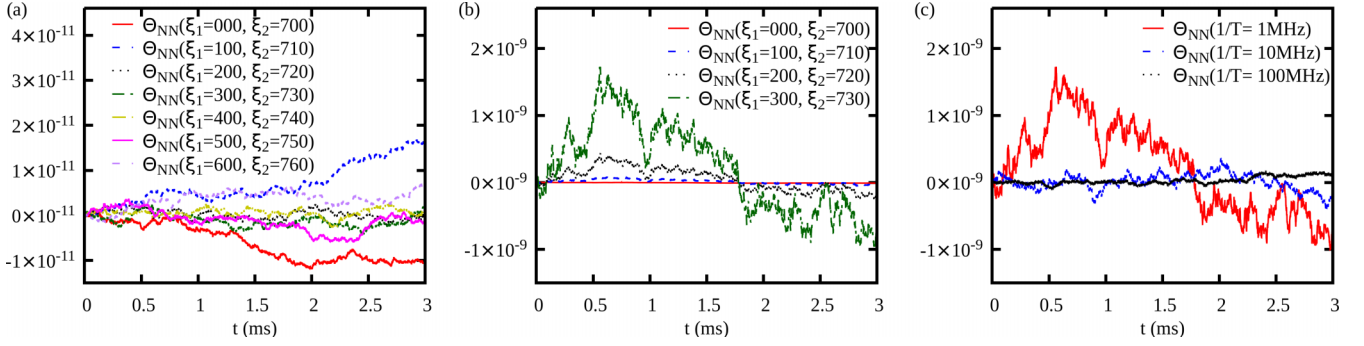


FIG. 7. Autocorrelative intensity $\Theta_{\text{NN}}(t; \tau)$ of various noises with different sampling frequencies $1/T$ of the APD: (a) autocorrelative results of noises $\mathbf{N}(t, \sigma^2, \xi_1)$ and $\mathbf{N}(t, \sigma^2, \xi_2)$ with different seeds ξ_1 and ξ_2 at $\text{SNR}^* = -18.6$ dB and $1/T = 1$ MHz, (b) autocorrelative results of noises $\mathbf{N}(t, \sigma^2, \xi_1 = 0)$ and $\mathbf{N}(t, \sigma^2, \xi_2 = 700)$ at sampling frequency $1/T = 1$ MHz with different SNR^* , and (c) autocorrelative results of noises $\mathbf{N}(t, \sigma^2, \xi_1 = 0)$ and $\mathbf{N}(t, \sigma^2, \xi_2 = 700)$ at $\text{SNR}^* = -18.6$ dB with different sampling frequencies $1/T$.

The measured results along with various types of noise with different sampling frequency $1/T$ are shown in Figs. 6 and 8. On this basis we compare the sensitivity and the stability (robustness) of the two schemes.

A. Signal-to-noise rate

Herein we use a general definition of SNR with voltage magnitudes of signals and noises in the WVA scheme,

$$\text{SNR} = 20 \log_{10} \frac{\max[V_I(t)]}{\max[V_N(t)]} = 20 \log_{10} \frac{\max[I_1^{\text{out}}(t)]}{\max[\mathbf{N}(t)]}, \quad (18)$$

where $\max[I(t)]$ and $\max[\mathbf{N}(t)]$ represent the maximum amplitude of the signal and the noise, respectively. The voltage magnitude $V_I(t) = \mathcal{K}I_1^{\text{out}}(t)$ is proportional to the amplitude of the signal $I_1^{\text{out}}(t)$ and the voltage magnitude $V_N(t) = \mathcal{K}\mathbf{N}(t)$ is proportional to the amplitude of the noise $\mathbf{N}(t)$, where the factor \mathcal{K} represents the coefficient of photoelectric conversion of the APD. Note that the SNR may not be well defined, due to $\max[\mathbf{N}(t)]$ increasing without bound as the number of samples is increased. Note that Fig. 9(a) indicates that the value of $\max[\mathbf{N}(t)]$ varies very little in the sampling frequency $1/T$ range of 1–100 MHz. Thus, we neglect this uncertainty of the SNR and calculate the SNR with the value of $\max[\mathbf{N}(t)]$ at $1/T = 10$ MHz. Take the example shown in Fig. 9(a), which gives $\text{SNR} = 20 \times \log_{10} \frac{1.40 \times 10^{-4}}{3.70 \times 10^{-5}} = 11.5$ dB. The numerical results in the WVA scheme with various kinds of noise are presented in Table II.

For the measurements with the AWVA technique, we define the sensitivity SNR^* as an intermediate step in the AWVA scheme and the sensitivity SNR^* is obtained by

$$\text{SNR}^* = 20 \times \log_{10} \frac{\max[I_{21}^{\text{out}}(t)]}{\max[\mathbf{N}(t)]}. \quad (19)$$

In the WVA scheme, the position of noise in the optical path has no effect on the calculation of SNR in our simulation, because there is only a single optical path in the WVA scheme. However, in the AWVA scheme, it is worth noting that the 50:50 beam splitter (shown in Fig. 2) will reduce the strength of the signal and introduce vacuum noise. Thus, where the noise appears will lead to the different values of SNR^* . When the noise is assumed to occur only in the optical path before the BS element, the value of SNR^* is equal to the value of SNR. Note that the relationship $\text{SNR}^* = \text{SNR}$ is true when we neglect the vacuum noise. This is the reason why a bright laser beam must be used; in that case the vacuum noise is small compared to the shot noise. In general, vacuum noise introduced by the BS element will cause $\text{SNR}^* > \text{SNR}$. When the noise is assumed to occur only in the optical path after the BS element, the value of SNR^* is reduced and $\text{SNR}^* = 0.5 \text{SNR}$. In addition, the value of SNR^* will be obtained at the range $0.5 \text{SNR} < \text{SNR}^* < \text{SNR}$ when the noises occur throughout the optical path in the AWVA scheme. In this paper, in order to highlight the advantages of the scheme, we investigate the lowest $\text{SNR}^* = 0.5 \text{SNR}$, because the lower the SNR^* is, the harder it is to detect a useful signal. In addi-

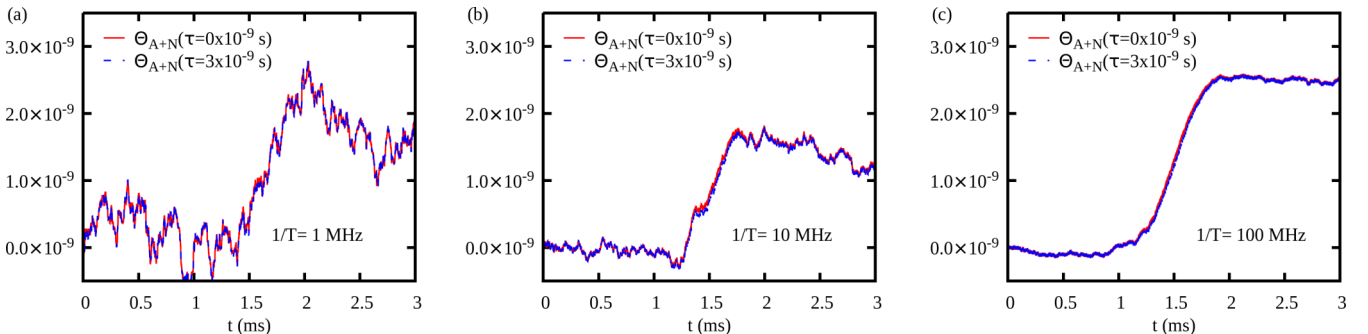


FIG. 8. Simulation results of the autocorrelative intensity Θ in the AWVA scheme noises $\mathbf{N}(t, \sigma^2, \xi_1 = 0)$ and $\mathbf{N}(t, \sigma^2, \xi_2 = 700)$ at $\text{SNR}^* = -18.6$ dB with different sampling frequencies: (a) $1/T = 1$ MHz, (b) $1/T = 10$ MHz, and (c) $1/T = 100$ MHz.

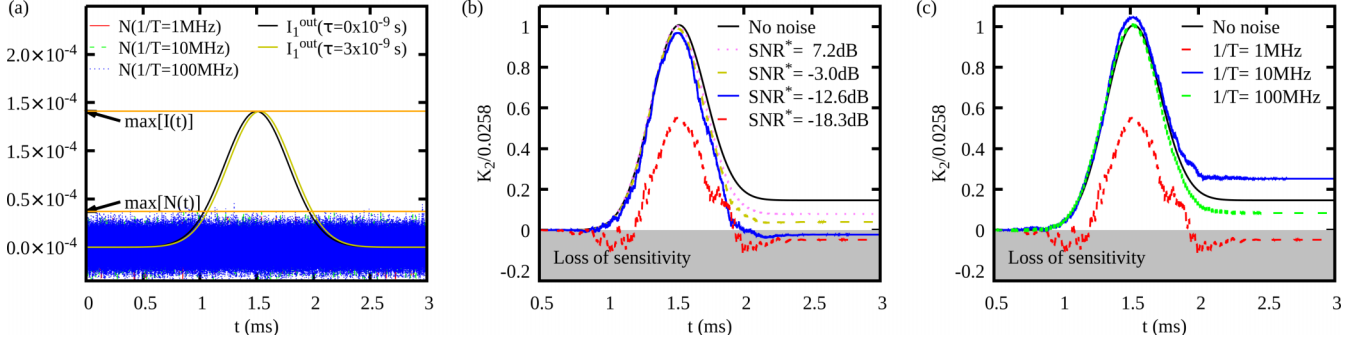


FIG. 9. Examples of estimating the SNR and the sensitivity the maximum sensitivity K_2^M : (a) example of estimating the SNR in the WVA scheme under Gaussian white noise $\mathbf{N}(t, \sigma^2 = 10^{-11}, \xi = 0)$ with different sampling frequencies, (b) dependence of the sensitivity with different SNR* on the integral time t under the noises $\mathbf{N}(t, \sigma^2, \xi_1 = 0)$ and $\mathbf{N}(t, \sigma^2, \xi_2 = 700)$ at sampling frequency $1/T = 1$ MHz, and (c) dependence of the sensitivity with different sampling frequencies $1/T$ on the integral time t under the noises $\mathbf{N}(t, \sigma^2, \xi_1 = 0)$ and $\mathbf{N}(t, \sigma^2, \xi_2 = 700)$ at SNR* = -18.6 dB. The gray band represents the measurements failing to effectively detect the final signal.

tion, by comparing the results with larger SNR* to the results with SNR* = 0.5 SNR in the AWVA scheme, our simulation can also model the effect of noise before the beam splitter. The results will be discussed in Sec. IV C.

Note that the relationship $\Theta_{A+N}(\tau) = \Theta_A(\tau)$ is only true if the integral time is infinite in Eq. (14). On the other hand, the sampling time (corresponding to the integral time) is finite and the pseudorandom number generator cannot generate truly random numbers. Thus, the various types of noise will affect the value of Θ and cause uncertainty in estimating the sensitivity of the scheme with the AWVA technique. In addition, the analysis of the sensitivity to various types of noise and the discussion of comparison with these results in the WVA scheme are given in the next section.

B. Sensitivity with the standard error

In order to calculate the sensitivity in the two schemes, we perform the simulation with both schemes with the time shift τ . In the WVA scheme, the sensitivity is defined as

$$K_1 = \frac{\Delta(\delta t)}{\Delta(\tau)} = \frac{\delta t_\tau - \delta t_0}{\tau}, \quad (20)$$

where the peak value shift δt_0 of the temporal pointer and its standard error E_{t_0} represent the results with the time shift $\tau = 0$ s. The peak value shift δt_τ of the temporal pointer and its standard error E_{t_τ} are obtained by fitting the Gaussian profile of the signal $I_1^{\text{out}}(t, \tau)$ with the least-squares method. Then the statistical error E_1 for estimating the value of K_1 can be calculated from Eq. (20) with the law of error propagation $E_1 = (|E_{t_\tau}| + |E_{t_0}|)/\tau$. Finally, the sensitivity K_1 with its statistical error E_1 under different simulation conditions are shown in Tables II and IV.

Note that the quantities measured in the AWVA scheme are the values of Θ ; therefore, the sensitivity in the AWVA scheme is defined as

$$K_2(t) = \frac{\Delta[\Theta(t; \tau)]}{\Delta(\tau)} = \frac{\Theta_0 - \Theta_\tau}{\tau}, \quad (21)$$

where Θ_τ represents the result $\Theta_{A+N}(t; \tau)$ calculated from Eq. (15) and Θ_0 represents the initial value of the measurement without the time shift τ and can be calculated from the

data I_{22+N}^{out} on APD2 in Fig. 2:

$$\Theta_0 = \int_0^t I_{22+N}^{\text{out}}(t') I_{22+N}^{\text{out}}(t') dt'. \quad (22)$$

Note that the sensitivity $K_2(t)$ depends on the scope of time integral t . The dependence of the sensitivity on t with various types of noise is shown in Figs. 9(b) and 9(c) and we can find that the maximum sensitivity K_2^M is achieved when integrated to $t = 1.5$ ms. In addition, we neglect the standard error of K_2^M , since Θ can be estimated by using a high-vertical-resolution oscilloscope. We show the maximum sensitivity K_2^M without standard errors in Tables III and V. In this paper we define the central value \bar{K}_2 with its statistical error E_2 in the AWVA scheme, which is created by calculating the seven statistical averages of K_2^M with different measurements:

$$\bar{K}_2 = \sum_{i=1}^n K_2^M(i)/n, \quad E_2 = \max\{|\bar{K}_2 - K_2^M(i)|\}, \quad (23)$$

where the $K_2^M(i)$ represents the result of the i th measurement with the different value of ξ , n represents the total number of measurements, and $n = 7$. For different simulation conditions, the central value \bar{K}_2 with its statistical error E_2 in the AWVA scheme is displayed in Tables III and V.

To compare the sensitivity in the two schemes, we further normalize them with their corresponding theoretical results in Figs. 10 and 11. Note that when the value of the sensitivity $K < 0$, corresponding to the loss of sensitivity area, the measurement is invalid. The central value \bar{K}_2 with its statistical error E_2 in the AWVA scheme is displayed as the red data points with an error bar in Figs. 10 and 11.

C. Effects of Gaussian noise with different SNRs

Figure 6 displays the results in the two schemes under Gaussian white noise with different SNRs. In addition, the corresponding results of the sensitivity are shown in Tables II and III. Combining the results of the normalized sensitivity in Fig. 10, we arrive at the following summaries of the effects of noises in the two schemes.

(i) In general, the AWVA scheme outperforms the WVA scheme, because the statistical error of the normalized

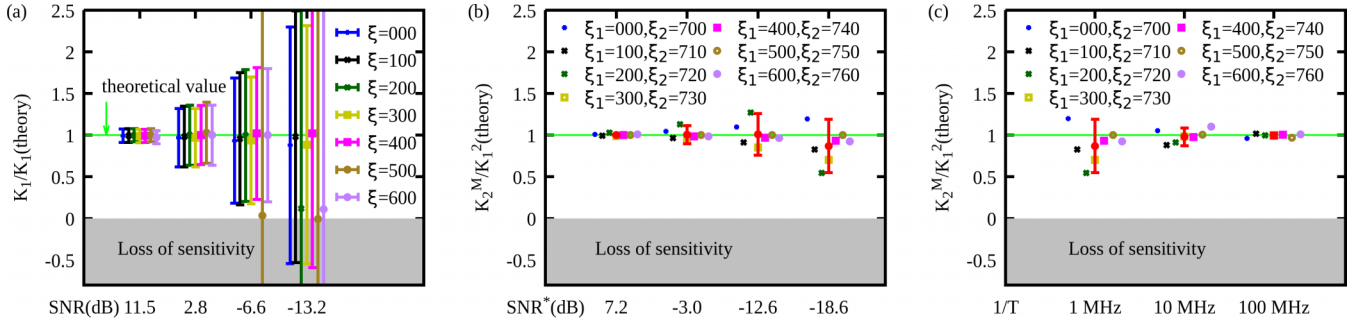


FIG. 10. Normalized sensitivity in the WVA scheme and in the AWVA scheme under Gaussian noises with different SNRs and sampling frequencies: (a) normalized sensitivity in the WVA scheme under noises $N(t, \sigma^2, \xi)$ with different SNRs, (b) normalized sensitivity in the AWVA scheme under noises $N(t, \sigma^2, \xi_1)$ and $N(t, \sigma^2, \xi_2)$ at sampling frequency $1/T = 1$ MHz with different SNR, and (c) normalized sensitivity in the AWVA scheme under noises $N(t, \sigma^2, \xi_1)$ and $N(t, \sigma^2, \xi_2)$ at SNR = -18.6 dB with different sampling frequencies $1/T$. The gray band represents the measurements failing to effectively detect the final signal. The red data points with the error bar represent the final results of seven statistical averages in the AWVA scheme.

sensitivity in the AWVA scheme is much smaller than that in the WVA scheme at the same level of SNR. Note that our results may be obtained by assuming that the time resolution and the vertical resolution of the oscilloscope can meet the requirements of our scheme, where the vertical resolution of the oscilloscope limits the accuracy of the value of Θ . On the other hand, the signal processing modules (Fig. 3) do not need to be implemented in hardware if the weak measurement does not meet the real-time measurement and this process may generate other kinds of noise. Thus, the results of Θ can be calculated mathematically after the measurement from the collected data on APD1 and APD2 of the scheme in Fig. 2.

(ii) There is no doubt that the intensity of noise significantly affects the results in both schemes. As shown in Fig. 10, the statistical errors of K_1 and \bar{K}_2 increase when the SNR is smaller. However, when the SNR is smaller than -6.6 dB, the central values of the measurement under noise $N(\text{SNR} = -6.6 \text{ dB}, \xi = 500)$, $N(\text{SNR} = -13.2 \text{ dB}, \xi = 300)$, $N(\text{SNR} = -13.2 \text{ dB}, \xi = 500)$, and $N(\text{SNR} = -13.2 \text{ dB}, \xi = 600)$ deviate greatly from the theoretical values in the WVA scheme. In addition, the measurements under noise at SNR = -13.2 dB in the WVA scheme are invalid due to the error bars extending into the loss of sensitivity area. Meanwhile, under the strong noise with negative-decibel SNR, the scheme with the AWVA technique

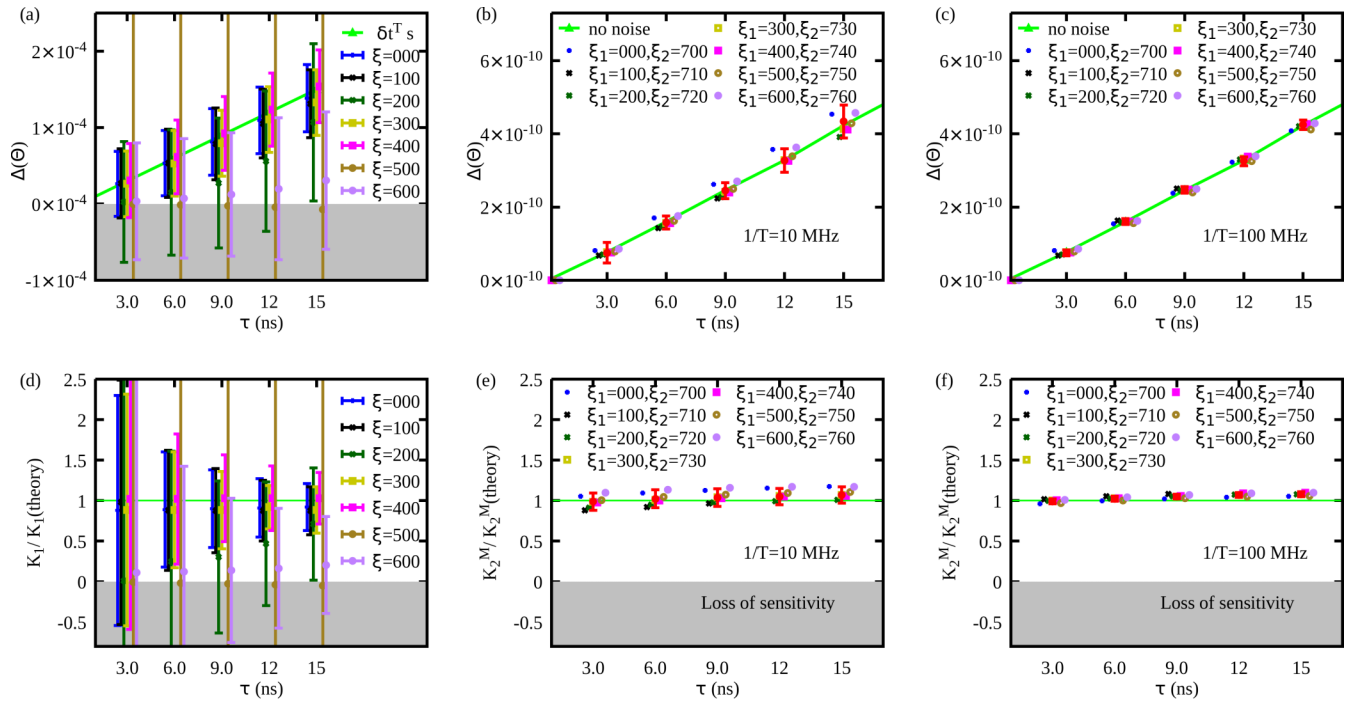


FIG. 11. Shifts $\Delta(\delta t)$ as well as (a)–(c) shifts $\Delta(\Theta)$ and (d)–(f) corresponding sensitivity with respect to the coupling strength τ under the Gaussian noise with SNR = -13.2 dB. Results are shown (a) and (d) under noises $N(t, \sigma^2, \xi)$ with different seeds ξ in the WVA scheme, (b) and (e) at sampling frequency $1/T = 10$ MHz under noises $N(t, \sigma^2, \xi_1)$ and $N(t, \sigma^2, \xi_2)$ with different seeds ξ_1 and ξ_2 in the AWVA scheme, and (c) and (f) at sampling frequency $1/T = 100$ MHz under noises $N(t, \sigma^2, \xi_1)$ and $N(t, \sigma^2, \xi_2)$ with different seeds ξ_1 and ξ_2 in the AWVA scheme. The red data points with the error bar represent the final results of seven statistical averages in the AWVA scheme.

gives more accurate results with smaller statistical errors than the scheme with the WVA technique.

(iii) Note that we obtain $\text{SNR}^* = 0.5 \text{ SNR}$ in the AWVA scheme by assuming that noise occurs after the beam splitter. When the noises occur throughout the optical path, the value of SNR^* will be obtained in the range $0.5 \text{ SNR} < \text{SNR}^* < \text{SNR}$. As shown in Fig. 10, the results corresponding to $0.5 \text{ SNR} < \text{SNR}^* < \text{SNR}$ are equivalent to shifting the curve to the right and lead to a smaller error bar compared to the results with $\text{SNR}^* = 0.5 \text{ SNR}$. Therefore, the AWVA scheme outperforms the WVA scheme no matter where the noise appears.

In conclusion, the advantage of the scheme with the AWVA technique is more obvious when the SNR is lower. Note that the statistical errors in the AWVA scheme get larger when the SNR is lower. Therefore, there is also a lower limit (corresponding to the minimum SNR) to how effective the AWVA scheme can be measured.

D. Effects of sampling frequency

In this paper we only investigate the influence of the sampling frequency $1/T$ on estimating the autocorrelative intensity Θ in the AWVA scheme due to the estimation of Θ strongly depending on the sampling frequency. In Sec. III the influence of the different sampling frequency $1/T$ on the autocorrelative intensity Θ_{NN} of noises was discussed. Figure 7(c) indicates that increasing the sampling frequency gets a lower Θ_{NN} . The effects of the different sampling frequencies on the autocorrelative intensity Θ_{A+N} of noises and the sensitivity in the AWVA scheme are shown in Table III and Fig. 10(c). Predictably, increasing sampling frequency $1/T$ can dramatically enhance the AWVA scheme's robustness.

It is worth noting that the upper limit of the sampling frequency $1/T$ is set at 100 MHz. There are two reasons for the choice in our simulation. One is that the results with $1/T = 100$ MHz are obviously better than the results with $1/T = 10$ MHz. In addition, our simulation with $1/T = 1000$ MHz on SIMULINK takes a prohibitively long time. Therefore, the simulation with a larger $1/T = 100$ MHz is unnecessary. Another reason is that, in order to achieve sampling accuracy, the realistic sampling frequency normally needs to reach 3–10 times the theoretical sampling frequency according to the Nyquist theorem [53]. The upper limit of sampling frequency is bound by the APD or analog-to-digital conversion. In addition, the sampling frequency $1/T$ set in this paper can be realized in the current Si or InGaAs Avalanche Photodetectors from Thorlabs.² Furthermore, it is difficult to guarantee that the time resolution ($1/T$) and the vertical resolution of the oscilloscope meet the requirements at the same time since the vertical resolution must be high enough to detect the shift of Θ .

E. Effects of coupling strength

In the two schemes for measuring the time shifts τ induced by a birefringent crystal, the time shift τ serves as the coupling

strength in the weak measurements. Next we will show the results with the two schemes at different coupling strengths τ . Note that this discussion is necessary because the two schemes can be transformed to measure other physical quantities. In Fig. 11 we show the results of δt in the WVA scheme and the shift of $\Theta(t = 1.5 \text{ ms})$ in the AWVA scheme, as well as their corresponding sensitivities, under the noise $\mathbf{N}(t, \sigma^2 = 4.0 \times 10^{-7})$ with $\text{SNR} = -13.2 \text{ dB}$. Note that the sensitivities K_1 and \bar{K}_2 have been normalized to highlight the deviation from the theoretical values. Figure 11 shows the deviations of the results in the two schemes from the theoretical value. We arrive at the following summaries of the effects of the coupling strength in the two schemes.

(i) Figures 11(a)–(c) display the shifts $\Delta(\delta t)$ in the WVA scheme and the shifts $\Delta(\Theta)$ in the AWVA scheme dependence of the coupling strength τ . Under the same noise with $\text{SNR} = -13.2 \text{ dB}$, the measurements with their error bars in the WVA scheme extending into the loss of sensitivity area are invalid, while all the measurements in the AWVA scheme give valid results with statistical errors. In addition, the central values of measuring $\Delta(\Theta)$ in the AWVA scheme agree with the theoretical results in the absence of noise. Nevertheless, the central values of measuring $\Delta(\delta t)$ in the WVA scheme deviate greatly from the theoretical values. In addition, the magnitudes of the statistical errors in the WVA scheme are independent of the coupling strength τ , which is easy to verify when discarding the measurements with the noise $\mathbf{N}(\sigma = 10^{-5}, \xi = 500)$ and $\mathbf{N}(\sigma = 10^{-5}, \xi = 600)$. In contrast, the magnitudes of the error bars in the AWVA scheme get bigger when the coupling strength τ increases.

(ii) Figures 11(d)–(f) display the normalized dependence of sensitivities K_1 and \bar{K}_2 of the coupling strength τ . The results in the WVA scheme indicate that the statistical errors of estimating K_1 get smaller when the coupling strength τ increases, while results in the AWVA scheme indicate that the statistical errors of estimating \bar{K}_2 are independent of the coupling strength τ . Furthermore, if the experimental conditions permit multiple measurements, the measurements where the central value deviates greatly from the theoretical value can be eliminated to obtain the results with smaller error bars.

(iii) Figures 11(b) and 11(e) ($1/T = 10$ MHz) and Figs. 11(c) and 11(f) ($1/T = 100$ MHz) show the influence of the sampling frequency on the results in the AWVA scheme. There is little deviation between the central value and the theoretical value with sampling frequency $1/T = 100$ MHz. Therefore, increasing the sampling frequency can enhance the robustness of detecting the change of the coupling strengths τ .

In conclusion, the scheme with the WVA technique is superior to the scheme with the AWVA technique when the coupling strength $\tau > 1.5 \times 10^{-8} \text{ s}$. On the other hand, the advantage of the scheme with the AWVA technique is more obvious when the coupling strength is lower and the sampling frequency is higher.

F. Measurements with different random seeds

So far, the previous results and discussion have been based on the assumption that the thermal noise and shot noise of the detection may not cause the different series of noise detected

²Thorlabs offers Menlo Systems' APD310 variable-gain, high-sensitivity avalanche photodetector, which offers high-speed response up to 1 GHz [54].

TABLE I. Numerical average results (dimensional quantities in unit of s) of the multiple measurement time shift $\tau = 3.0 \times 10^{-9}$ s under Gaussian noise with different SNRs.

SNR	$1/T$	$\delta\bar{t}_0(\pm\bar{E}_{t0})$	$\delta\bar{t}_\tau(\pm\bar{E}_{t\tau})$	$\Delta(\delta\bar{t})$	$\bar{K}_1(\pm\bar{E}_1)/1.0 \times 10^3$
11.5	1	$8.97 \times 10^{-7} (\pm 2.09 \times 10^{-6})$	$3.09 \times 10^{-5} (\pm 2.30 \times 10^{-6})$	$3.00 \times 10^{-5} (\pm 4.39 \times 10^{-6})$	$1.000(\pm 0.146)$
2.8	1	$4.02 \times 10^{-6} (\pm 9.58 \times 10^{-6})$	$3.38 \times 10^{-5} (\pm 1.07 \times 10^{-5})$	$2.98 \times 10^{-5} (\pm 2.03 \times 10^{-5})$	$0.993(\pm 0.676)$
-6.6	1	$1.84 \times 10^{-4} (\pm 1.07 \times 10^{-3})$	$2.11 \times 10^{-4} (\pm 1.06 \times 10^{-3})$	$2.70 \times 10^{-5} (\pm 2.13 \times 10^{-3})$	$0.900(\pm 71.00)$
-13.2	1	$1.59 \times 10^{-4} (\pm 1.27 \times 10^{-3})$	$1.76 \times 10^{-4} (\pm 1.27 \times 10^{-3})$	$1.70 \times 10^{-5} (\pm 2.54 \times 10^{-3})$	$0.566(\pm 84.66)$
SNR	$1/T$	$\bar{\Theta}_0(\pm\bar{E}_{c0})$	$\bar{\Theta}_\tau(\pm\bar{E}_{c\tau})$	$\Delta\bar{\Theta}$	$\bar{K}_2(\pm\bar{E}_2)/0.0258$
11.5	1	$1.2450 \times 10^{-9} (\pm 1.41 \times 10^{-11})$	$1.1672 \times 10^{-9} (\pm 1.45 \times 10^{-11})$	$7.78 \times 10^{-11} (\pm 2.86 \times 10^{-11})$	$1.005(\pm 0.369)$
2.8	1	$1.2426 \times 10^{-9} (\pm 1.41 \times 10^{-10})$	$1.1646 \times 10^{-9} (\pm 1.43 \times 10^{-10})$	$7.80 \times 10^{-11} (\pm 2.84 \times 10^{-10})$	$1.008(\pm 3.669)$
-6.6	1	$1.2235 \times 10^{-9} (\pm 5.92 \times 10^{-10})$	$1.1452 \times 10^{-9} (\pm 5.96 \times 10^{-10})$	$7.83 \times 10^{-11} (\pm 1.19 \times 10^{-09})$	$1.012(\pm 15.37)$
-13.2	1	$1.5567 \times 10^{-9} (\pm 2.17 \times 10^{-09})$	$1.4886 \times 10^{-9} (\pm 1.77 \times 10^{-09})$	$6.81 \times 10^{-11} (\pm 3.94 \times 10^{-09})$	$0.880(\pm 50.90)$
-13.2	10	$1.5728 \times 10^{-9} (\pm 7.52 \times 10^{-10})$	$1.4961 \times 10^{-9} (\pm 7.46 \times 10^{-10})$	$7.67 \times 10^{-11} (\pm 1.50 \times 10^{-09})$	$0.991(\pm 19.38)$
-13.2	100	$1.2764 \times 10^{-9} (\pm 3.67 \times 10^{-10})$	$1.1993 \times 10^{-9} (\pm 3.67 \times 10^{-10})$	$7.71 \times 10^{-11} (\pm 7.34 \times 10^{-10})$	$0.996(\pm 9.483)$

on APD1 and APD2 in the AVWA scheme. Therefore, the shift $\Delta\bar{\Theta}$ and sensitivity K_2 were calculated from the data for $\bar{\Theta}(\tau = 0)$ and $\bar{\Theta}(\tau)$ with the same ξ . In other words, the noise is the same when $\bar{\Theta}(\tau = 0)$ and $\bar{\Theta}(\tau)$ are measured. Meanwhile, we calculate $\Delta(\delta\bar{t})$ from the data for $\delta\bar{t}_0$ and $\delta\bar{t}_\tau$ with the same ξ . Note that these measurements can only be completed under special experimental conditions. Further, we use the data with the different ξ to estimate the shifts $\Delta(\delta\bar{t})$ and $\Delta\bar{\Theta}$. In particular, the results of the measurements with different random seeds were calculated and are shown in Table I, where the average results $\delta\bar{t}_0(\pm\bar{E}_{t0})$, $\delta\bar{t}_\tau(\pm\bar{E}_{t\tau})$, $\bar{\Theta}_0(\pm\bar{E}_{c0})$, and $\bar{\Theta}_\tau(\pm\bar{E}_{c\tau})$ of multiple measurements are re-defined as

$$\delta\bar{t}_0 = \sum_{i=1}^n \delta t_0(i)/n, \quad \bar{E}_{t0} = \max\{|\delta\bar{t}_0 - \delta t_0(i)|\}, \quad (24)$$

$$\delta\bar{t}_\tau = \sum_{i=1}^n \delta t_\tau(i)/n, \quad \bar{E}_{t\tau} = \max\{|\delta\bar{t}_\tau - \delta t_\tau(i)|\}, \quad (25)$$

$$\bar{\Theta}_0 = \sum_{i=1}^n \Theta_0(i)/n, \quad \bar{E}_{c0} = \max\{|\bar{\Theta}_0 - \Theta_0(i)|\}, \quad (26)$$

$$\bar{\Theta}_\tau = \sum_{i=1}^n \Theta_\tau(i)/n, \quad \bar{E}_{c\tau} = \max\{|\bar{\Theta}_\tau - \Theta_\tau(i)|\}, \quad (27)$$

where (i) represents the result of the i th measurement with the different value of ξ , n represents the total number of measurements, and $n = 7$. Then the corresponding shifts $\Delta(\delta\bar{t})$ and $\Delta\bar{\Theta}$ are obtained by the relationships $\Delta(\delta\bar{t}) = \delta\bar{t}_\tau - \delta\bar{t}_0$ and $\Delta\bar{\Theta} = \bar{\Theta}_0 - \bar{\Theta}_\tau$. Furthermore, the sensitivity $\bar{K}_1(\pm\bar{E}_1)$ in the WVA scheme and the sensitivity $\bar{K}_2(\pm\bar{E}_2)$ can be calculated by

$$\bar{K}_1 = \delta\bar{t}/\tau, \quad \bar{E}_1 = (\bar{E}_{t0} + \bar{E}_{t\tau})/\tau, \quad (28)$$

$$\bar{K}_2 = \delta\bar{t}/\tau, \quad \bar{E}_2 = (\bar{E}_{c0} + \bar{E}_{c\tau})/\tau. \quad (29)$$

Finally, we display these average results of the multiple measurements with different random seeds in Table I. The simulation results show that the AVWA scheme with larger error bars has no advantage over the WVA scheme in the environment of weak noises with SNR = 11.5 and 2.8 dB

when the sampling frequency is set $1/T = 1$ MHz; however, the error bars can decrease when a larger sampling frequency is employed. When multiple measurements are completed under strong noises with SNR = -6.6 and -13.2 dB, the central value $\bar{K}_2/0.0258$ (0.0258 corresponding to the theoretical value without noise) is closer to the theoretical value 1 and the values of $\bar{E}_2/0.0258$ are much smaller than those of statistical errors $\bar{E}_1/1.0 \times 10^3$. In addition, the results of multiple measurements with a larger sampling frequency $1/T$ have smaller deviation of the central value $\bar{K}_2/0.0258$ from the theoretical value and statistical errors \bar{E}_2 . In general, when multiple measurements are completed under strong noises with a negative-decibel SNR, the AVWA scheme may have the potential to outperform the WVA scheme with a smaller deviation from the theoretical value and statistical errors. The AVWA technique is a kind of easily realized scheme that can adapt to strong noise for real-time estimation of unknown small evolution parameters.

V. CONCLUSION

We have performed a scheme with autocorrelative weak-value amplification for precision phase estimation. A simulated experiment for estimating the time shift with the standard weak-value amplification technique and the autocorrelative weak-value amplification technique has been derived under Gaussian white noise with different signal-noise-ratios. In addition, a new quality (pointer), namely, the autocorrelative intensity $\bar{\Theta}$, is defined in our scheme with the AVWA technique to estimate the small signal. Compared to fitting the shift of the Gaussian pointer with the standard WVA technique, measuring the shift of $\bar{\Theta}$ has the advantage of suppressing noise and the advantage of the scheme with the AVWA technique is more obvious when the SNR and the coupling strength are lower. Therefore, our results have demonstrated that the AVWA technique outperforms the standard WVA technique in the time domain even when the signal is submerged in noise (SNR < 0). The robustness suggests that the AVWA technique can be applied for a vast range of weak measurements in the time domain.

Note that we assumed that the contribution of all noise is Gaussian white noise in this paper. However, the real technical noise and environmental noise are far more complex than Gaussian white noise. In addition, in many areas of physics Gaussian noise has been replaced by colored noise (non-Gaussian) [27–30]. Therefore, the autocorrelative weak-value amplification technique under colored noises or real noises should be investigated in future work. In addition, our analysis pertains only to values of $\alpha = 0.01$ rad corresponding to a particular regime of near orthogonality of the initial and final states. This is because the value around 0.01 rad is the most relevant regime for high sensitivity of weak-value amplification [12,16,55]. However, it is worth further comparing the WVA scheme and the AWVA scheme with a different regime of near orthogonality. Furthermore, Hermite-Gaussian and Laguerre-Gaussian pointer states [56] and other nonclassical pointer states (squeezed vacuum and Schrödinger-cat states) [57] have shown their advantages in the WVA measurement over using the Gaussian beam profile. Certainly it is worth going beyond the Gaussian beam profile and comparing the WVA measurement and the AWVA measurement. Finally, we must admit that the precision and robustness of the AWVA technique depends on both the sampling frequency $1/T$ and the vertical resolution of the oscilloscope. Thus, our scheme needs further experimental verification.

The general definition of SNR in Eqs. (18) and (19) with voltage magnitudes of signals and noises can be replaced by Fisher information [26,41,46,47] in information theory. Fisher information is a way of calculating the fundamental limit of the minimum uncertainty for the parameter estimation and has been widely used to estimate the SNR in the standard weak measurement. Indeed, the SNR calculation based on Fisher information is more reasonable and investigation of the fundamental limit of the AWVA scheme is left for future work.

After completion of this work, we found that the AWVA technique can also be achieved on the weak measurement in the frequency domain. The quantity Θ can also be obtained mathematically by the integral of momentum. The work is in progress.

ACKNOWLEDGMENTS

This study was supported by the National Science Foundation of China (Grant No. 42220104002), MOST Special Fund from the State Key Laboratory of Geological Processes and Mineral Resources, and the China University of Geosciences (Grant No. MSFGPMR01-4). J.-H.H. acknowledges support from the China Scholarship Council (Grant No. 202206410063). A.C.D. acknowledges support from the EPSRC, Impact Acceleration Account (Grant No. EP/R511705/1).

APPENDIX A: OVERVIEW OF SIMULINK

SIMULINK, a MATLAB-based graphical programming environment, is widely used in automatic control and digital signal processing for multidomain simulation and model-based design. Its primary interface is a graphical block diagramming tool and a customizable set of block libraries [58]. For modeling, SIMULINK provides a graphical user interface for building

models as block diagrams. It includes a comprehensive library of predefined blocks to be used to construct graphical models of systems using drag-and-drop mouse operations. The user is able to produce an up-and-running model that would otherwise require hours to build in the laboratory environment. It offers tight integration with the rest of the MATLAB environment and can either drive MATLAB or be scripted from it. Therefore, SIMULINK and MATLAB can interact with each other through the MATLAB workspace. Normally, one can generate data or signal from Sources in SIMULINK or bring in data from the MATLAB workspace. Similarly, one can use sinks to visualize data or bring it back out into the MATLAB workspace. In this paper we used several blocks for modeling: the Random Number block with different variance, seed, and sampling time; the Sum block; the Product block; the Integrator block; the BusCreator block for creating a bus signal; and the Scope block for presenting the data and bringing it to the workplace of MATLAB. We will elaborate on our measurement scheme in the following Appendixes.

APPENDIX B: PREPARING FOR THE MOLDING ON SIMULINK

To simulate the WVA and AWVA schemes with the temporal pointer on SIMULINK in a realistic situation, the effects of Gaussian white noises with different SNRs on the two schemes are investigated first. In this paper we approximate the optical noise due to the instability of the light source, interference in the light path, thermal noise and shot noise of the detection, the partition noise (vacuum noise) due to the beam splitter, and noises from other unknown sources as Gaussian noise. We add the noise $\mathbf{N}(t, \sigma^2; \xi)$ into both the WVA scheme and the AWVA scheme. For the measurement with the WVA technique, one gets the final signal $I_{1+N}^{\text{out}}(t; \tau)$ under $\mathbf{N}(t, \sigma^2, \xi)$ as

$$I_{1+N}^{\text{out}}(t; \tau) = I_1^{\text{out}}(t; \tau) + \mathbf{N}(t, \sigma^2, \xi). \quad (\text{B1})$$

For the measurement with the AWVA technique, one gets the final signal $I_{21+N}^{\text{out}}(t; \tau)$ on APD1 and $I_{22+N}^{\text{out}}(t; \tau)$ on APD2 under $\mathbf{N}(t, \sigma^2, \xi_1)$ and $\mathbf{N}(t, \sigma^2, \xi_2)$, respectively:

$$I_{21+N}^{\text{out}}(t; \tau) = I_{21}^{\text{out}}(t; \tau) + \mathbf{N}(t, \sigma^2, \xi_1), \quad (\text{B2})$$

$$I_{22+N}^{\text{out}}(t; \tau) = I_{22}^{\text{out}}(t; \tau) + \mathbf{N}(t, \sigma^2, \xi_2). \quad (\text{B3})$$

Note that the signals $I_1^{\text{out}}(t; \tau)$, $I_{21}^{\text{out}}(t; \tau)$, and $I_{22}^{\text{out}}(t; \tau)$ represent the results without noises. Therefore, they can directly calculated by the definition in the main text:

$$I_1^{\text{out}}(t; \tau) = I_0 \frac{(\sin\alpha)^2}{(2\pi\omega^2)^{1/4}} e^{-(t-t_0-\delta t)^2/4\omega^2}, \quad (\text{B4})$$

$$I_{21}^{\text{out}}(t; \tau) = \frac{I_0}{2} \frac{(\sin\alpha)^2}{(2\pi\omega^2)^{1/4}} e^{-(t-t_0-\delta t)^2/4\omega^2}, \quad (\text{B5})$$

$$I_{22}^{\text{out}}(t; \tau) = \frac{I_0}{2} \frac{(\sin\alpha)^2}{(2\pi\omega^2)^{1/4}} e^{-(t-t_0)^2/4\omega^2}, \quad (\text{B6})$$

where I_0 is set equal to unity, ω is set as 0.0002, t_0 is set as 0.0015 s, and the angle for postselection is set at $\alpha = 0.01$ rad.

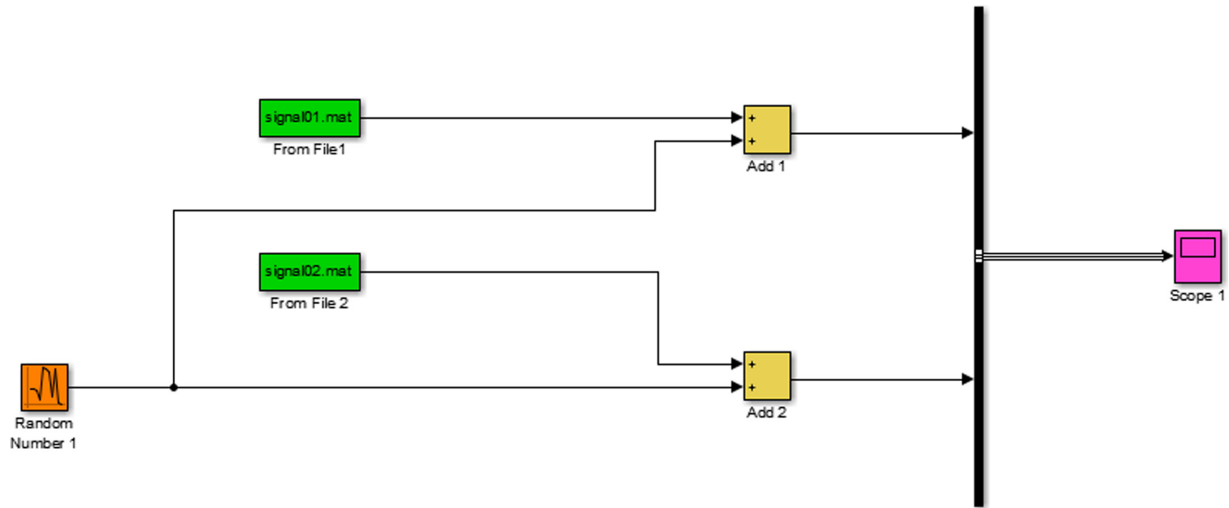


FIG. 12. Scheme of the WVA measurement in SIMULINK. The signal01.mat block and signal02.mat block represent the array of the signals $I_1^{\text{out}}(t; \tau)$ with different τ in the MATLAB workplace. The Random Number 1 block represents the random number generator. The Add 1 and Add 2 blocks represent adding inputs. The Scope 1 block represents the oscilloscope. The Bus Creator block combines a set of signals into a bus.

These functions can be easily implemented in MATLAB and used as the source or input in SIMULINK.

APPENDIX C: SCHEME FOR THE WVA MEASUREMENT

The scheme for the WVA measurement on SIMULINK is shown in Fig. 12. The signal01.mat block represents the array of the signals $I_1^{\text{out}}(t; \tau = 0 \text{ ns})$, while the signal02.mat block represents the array of the signals $I_1^{\text{out}}(t; \tau)$. The Random Number block generates normally distributed random numbers. We can generate a repeatable sequence using any Random Number block with the same non-negative seed and parameters. The seed resets to the specified value each time a simulation starts. By default, the block produces a sequence that has a mean of 0 and a variance of 1. The Bus Creator block combines a set of signals into a bus. To bundle a group of signals with a Bus Creator block, we set the block parameter of number of inputs to the number of signals in the group. The block displays the number of ports that we specify. We connect to the resulting input ports those signals that we want to group. In the main text, we discuss that the simulation results are dependent on the noise strength, the seed of the noise, and the sampling time. These features can be set by changing the parameters of the Random Number 1 blocks as shown in Fig. 13. Changing the value of Variance can set the strength of noises. Different values of Seed can generate different noises with different initial times. The sampling period of our system can be set by varying the value of the Sample time.

After determining the simulation conditions, we run our simulation and we can present the final signals on Scope 1 and save them as an array in the workplace of MATLAB. Then the data can be fitted as the Gaussian profile by Origin to estimate the shift of the mean value. Next we take the parameter in Fig. 13 as an example. By calculating the outputs $I_1^{\text{out}}(t; \tau = 0 \text{ ns})$ and $I_1^{\text{out}}(t; \tau = 3 \text{ ns})$ without noises and saving them as signal01.mat and signal02.mat arrays, the results of the

measurements $\tau = 0$ and 3 ns are shown in Fig. 14. Finally, data on Scope 1 can be saved in the workplace and fitted with a Gaussian profile in Origin. Figure 15 display the Gaussian fitting results of the measurement $\tau = 0$ ns and the measurement $\tau = 3$ under Gaussian noise with the seed equal to 600 at SNR equal to 11.5 dB. The shifts of the mean value can be directly read $\delta t_0(\pm E_{t0}) = -1.20 \times 10^{-6}(\pm 1.28 \times 10^{-6})$ and $\delta t_\tau(\pm E_{t\tau}) = 2.88 \times 10^{-5}(\pm 1.28 \times 10^{-6})$. By changing the values of the Variance and Seed, the simulation results with various SNRs and different ξ can be obtained and are displayed in Tables II and IV.

APPENDIX D: SCHEME FOR THE AWVA MEASUREMENT

The scheme for the AWVA measurement on SIMULINK is shown in Fig. 16. The signal1.mat, signal2.mat, Random Number 2, Random Number 3, Add 3, Add 4, Add 5, Add

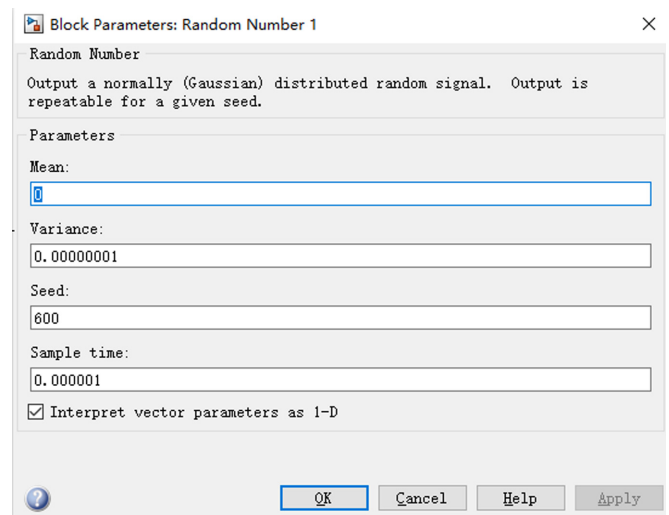


FIG. 13. Block parameters of Random Number 1.

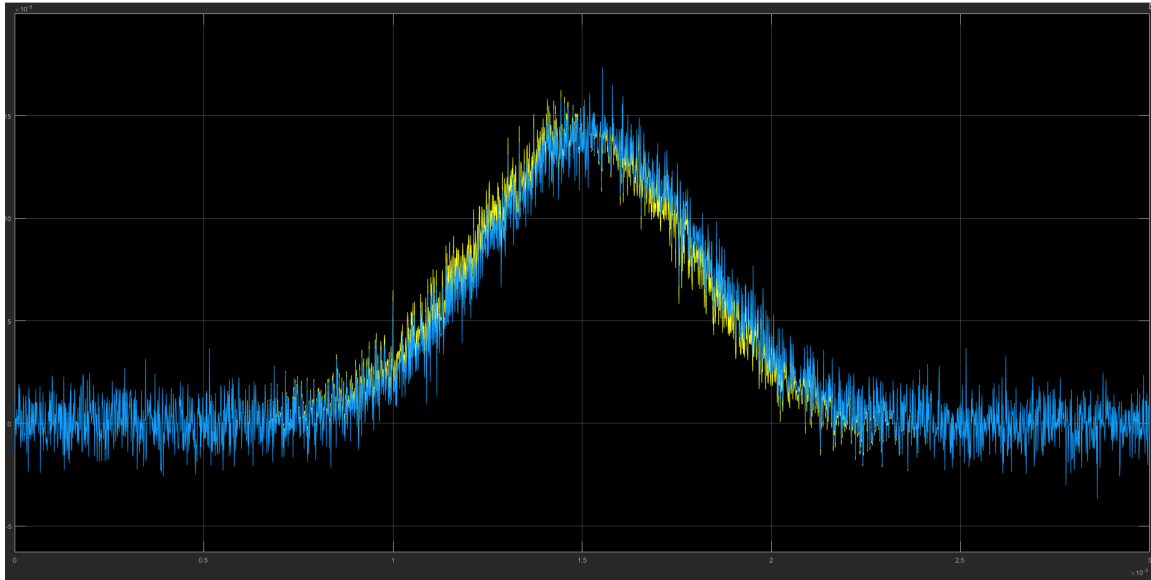


FIG. 14. Example of the display of Scope 1. The data are taken from the simulation of the measurement $\tau = 0$ ns and the measurement $\tau = 3$ under Gaussian noise with seed equal to 600 at SNR equal to 11.5 dB.

6, Scope 2, and Scope 3 blocks represent the same features as the scheme for the WVA measurement in Fig. 12. In addition, the Product 1 and Product 2 blocks output the result of multiplying two inputs: two scalars, a scalar and a nonscalar, or two nonscalars that have the same dimensions. The Integrator 1 and Integrator 2 blocks output the value of the integral of its input signal with respect to time. The signal1.mat block represents the array of the signals $I_{21}^{\text{out}}(t; \tau = 0$ ns), while the signal2.mat block represents the array of the signals $I_{22}^{\text{out}}(t; \tau)$. Note that the seeds in the Random Number 2 block and the Random Number 3 block need to be set at different values according to the discussion in the main text. By setting the seed equal to 000 in the Random Number 2 block and equal to 700 in the Random Number 3 block at SNR = 11.5 dB with sampling frequency $1/T = 1$ MHz as shown in Fig. 17, the signals $I_{21}^{\text{out}}(t; \tau)$ and $I_{22}^{\text{out}}(t; \tau)$ can be obtained from Scope 3 as displayed in Fig. 18 and the autocorrelative intensity Θ_{NN} with different τ can be obtained from Scope 2 as displayed in Figs. 19 and 20.

After determining the simulation conditions, we run our simulation; we can present the final signals on Scope 2 and Scope 3 and save them as an array in the workplace of MATLAB. Figure 19 displays the autocorrelative intensity Θ_{NN} of the measurement $\tau = 0$ ns and the measurement $\tau = 3$ ns under Gaussian noise with seed equal to 000 in the Random Number 2 block and seed equal to 700 in the Random Number 3 block at SNR = 11.5 dB. It can be found that the intensity Θ_{NN} can be directly read out from Scope 2. By changing the values of the Variance, Seed, and Sample time, the simulation results with various SNRs, different ξ_1 and ξ_2 , and sampling frequency can be obtained and displayed in Tables III, V and VI.

APPENDIX E: SIMULATION DATA FOR THE MAIN TEXT

To simulate the WVA measurements and AWVA measurements under hypothetical conditions, several simulations of both the WVA measurements and AWVA measurements are implemented.

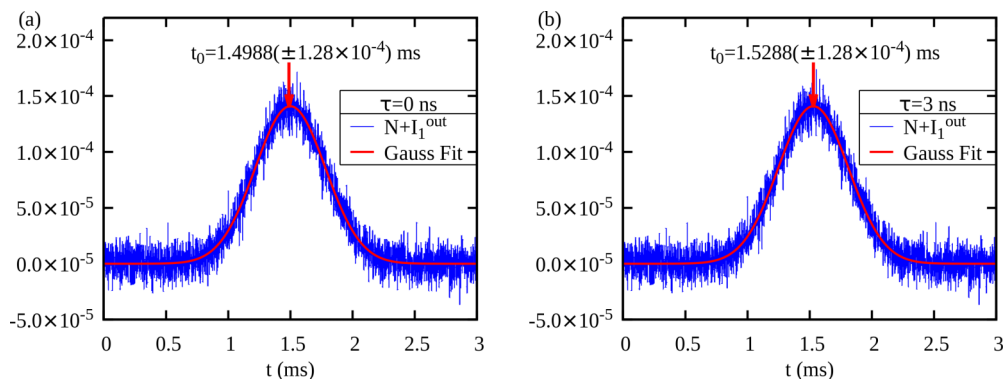


FIG. 15. Example of Gaussian fitting. The data are taken from the simulation of (a) the measurement $\tau = 0$ ns and (b) the measurement $\tau = 3$ under Gaussian noise with seed equal to 600 at SNR equal to 11.5 dB.

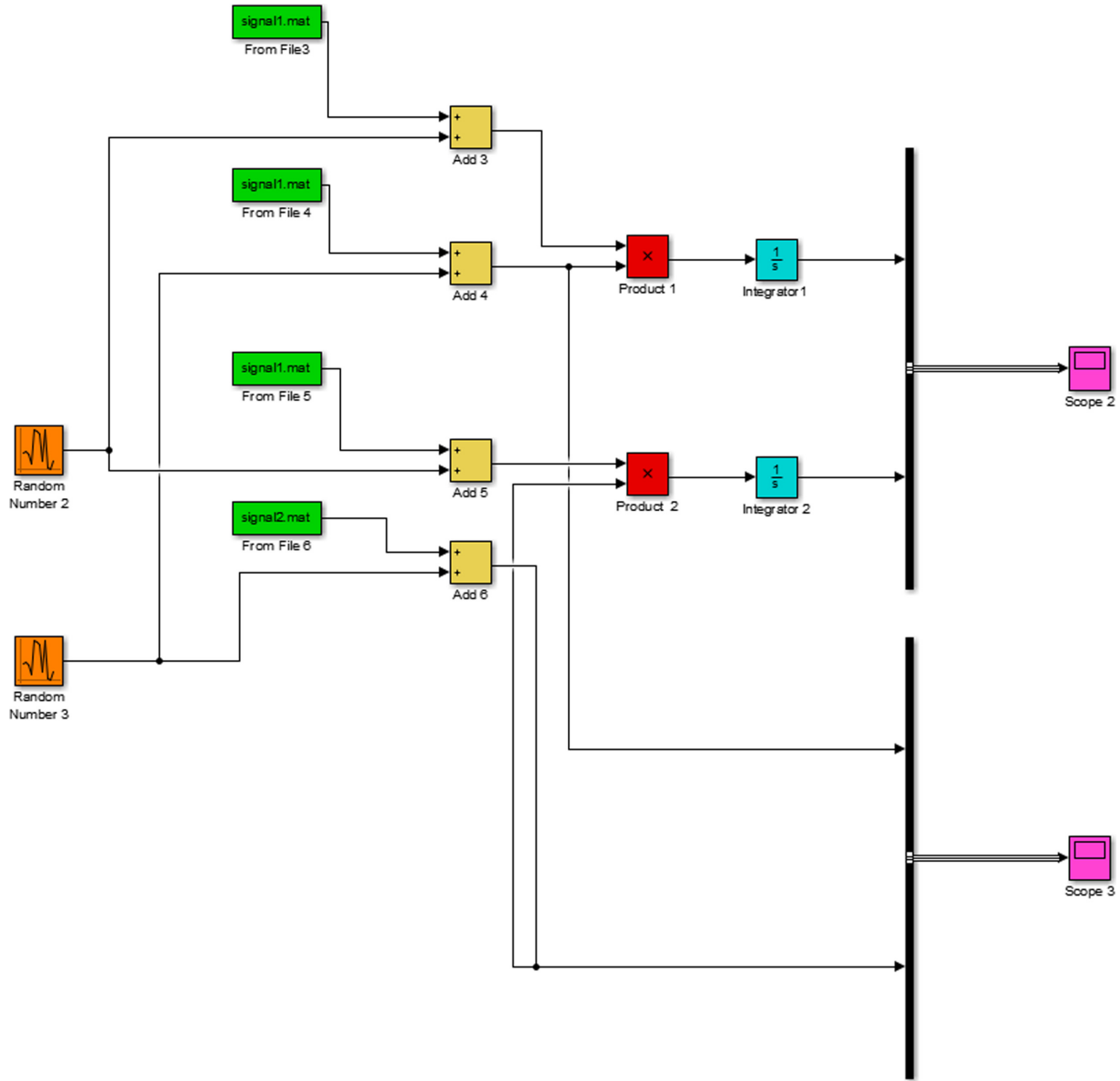


FIG. 16. Scheme of the AWVA measurement in SIMULINK. The `signal1.mat` block and `signal2.mat` block represent the array of signals $I_{21}^{\text{out}}(t; \tau)$ and $I_{22}^{\text{out}}(t; \tau)$ with different τ in the MATLAB workplace. The Random Number 2 and Random Number 3 blocks represent the random number generator. The Add 3, Add 4, Add 4, and Add 6 blocks represent adding inputs. The Product 1 and Product 2 blocks represent multiplying inputs. The Integrator 1 and Integrator 2 blocks represent multiplying inputs. The Scope 2 and Scope 3 blocks output the value of the integral of its input signal with respect to time. The Bus Creator block combines a set of signals into a bus.

(i) Figure 6 displays the simulation results in two schemes under Gaussian white noise with different SNRs. The sampling frequency is set at $1/T = 1$ MHz.

(ii) Table II shows the numerical results of measuring time shift $\tau = 3.0 \times 10^{-9}$ under Gaussian noise $\mathbf{N}(t, \xi)$ with different SNRs in the WVA scheme. The sampling frequency is set at $1/T = 1$ MHz.

(iii) Table III shows the numerical results of measuring the time shift $\tau = 3.0 \times 10^{-9}$ under Gaussian noises $\mathbf{N}(t, \sigma^2, \xi_1)$ and $\mathbf{N}(t, \sigma^2, \xi_2)$ with different SNRs and different sampling frequencies $1/T$ in the AWVA scheme.

(iv) Table IV shows the numerical results of measuring the different τ under the strong noise $\mathbf{N}(t, \xi)$ at $\text{SNR} = -13.2$ dB in the WVA scheme. The sampling frequency is set at $1/T = 1$ MHz.

(v) Table V shows the numerical results for measuring the different τ under the strong noises $\mathbf{N}(t, \sigma^2, \xi_1)$ and $\mathbf{N}(t, \sigma^2, \xi_2)$ at $\text{SNR} = -13.2$ dB in the AWVA scheme. The sampling frequency is set at $1/T = 10$ MHz.

(vi) Table VI shows the numerical results for measuring the different τ under the strong noises $\mathbf{N}(t, \sigma^2, \xi_1)$ and $\mathbf{N}(t, \sigma^2, \xi_2)$ at $\text{SNR} = -13.2$ dB in the AWVA scheme. The sampling frequency is set at $1/T = 100$ MHz.

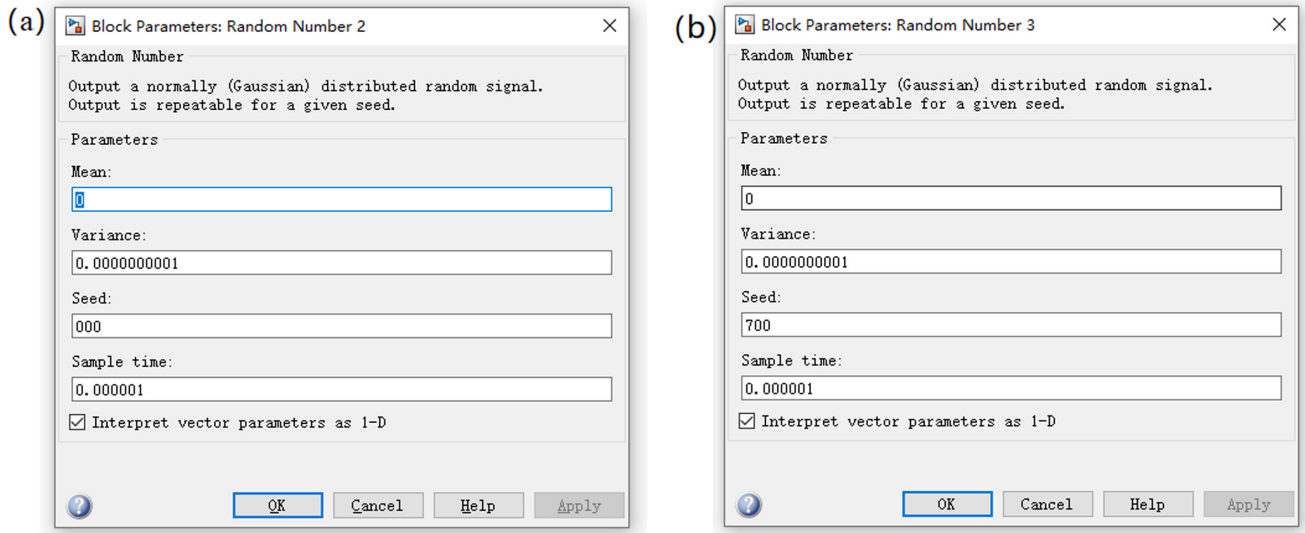


FIG. 17. Example of the parameter set of (a) the Random Number 2 block and (b) the Random Number 3 for the measurement $\tau = 0$ ns and the measurement $\tau = 3$ ns under Gaussian noise, respectively, with (a) seed equal to 000 in the Random Number 2 block and (b) seed equal to 700 in the Random Number 3 block at SNR equal to 11.5 dB.

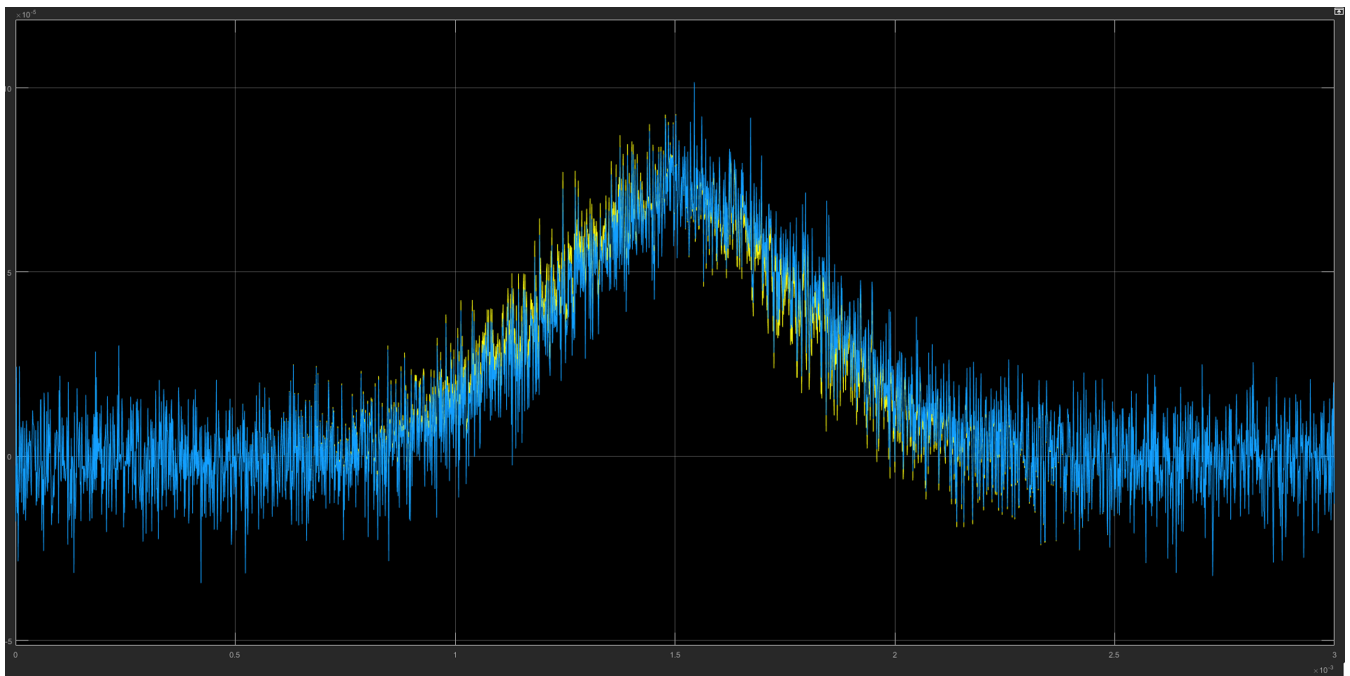


FIG. 18. Example of the display of Scope 3. The data are taken from the simulation of the measurement $\tau = 0$ ns and the measurement $\tau = 3$ ns under Gaussian noise with seed equal to 000 in the Random Number 2 block and seed equal to 700 in the Random Number 3 block at SNR equal to 11.5 dB.

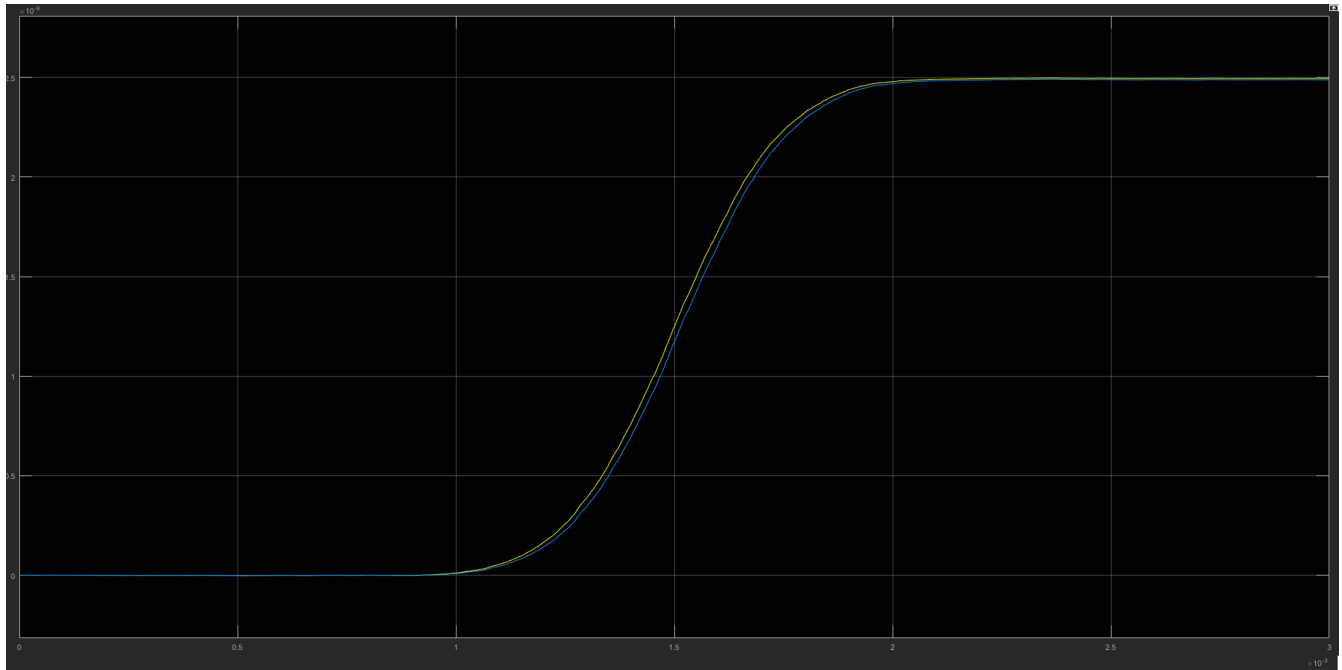


FIG. 19. Example of the display of Scope 2. The data are taken from the simulation of the measurement $\tau = 0$ ns and the measurement $\tau = 3$ ns under Gaussian noise with seed equal to 000 in the Random Number 2 block and seed equal to 700 in the Random Number 3 block at SNR equal to 11.5 dB.

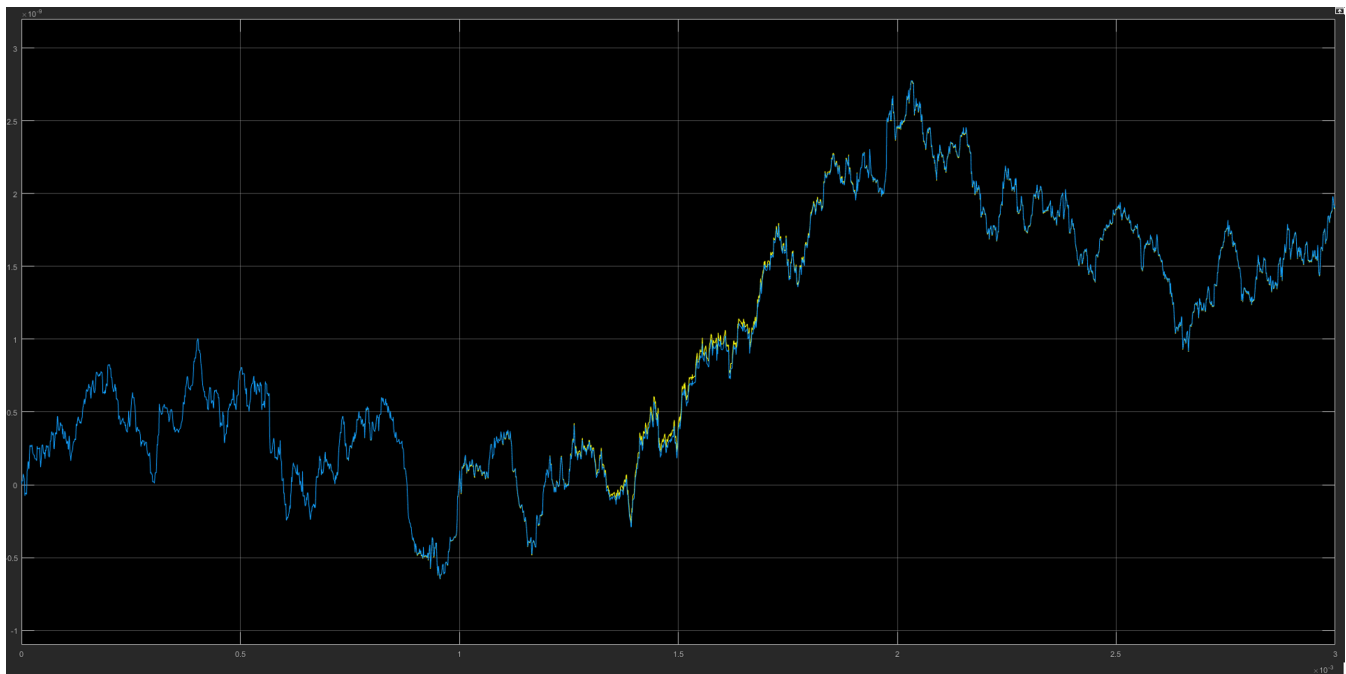


FIG. 20. Example of the display of Scope 2. The data are taken from the simulation of the measurement $\tau = 0$ ns and the measurement $\tau = 3$ ns under Gaussian noise with seed equal to 000 in the Random Number 2 block and seed equal to 700 in the Random Number 3 block at SNR equal to -13.2 dB.

TABLE II. Parameters and some characteristic numerical results (dimensional quantities in units of s) of measuring the time shift $\tau = 3.0 \times 10^{-9}$ under Gaussian noise with different SNRs in the WVA scheme. The contents E_{t_0} and E_{t_τ} in parentheses represent the standard error for estimating the time shifts δt_0 and δt_τ , respectively. Here $\mathbf{N}(\xi = 0)$, $\mathbf{N}(\xi = 100)$, \dots , $\mathbf{N}(\xi = 600)$ represent multiple measurements with different initial times.

SNR	Noise	$\delta t_0(\pm E_{t_0})$	$\delta t_\tau(\pm E_{t_\tau})$	$K_1(\pm E_1)$
	no noise	$0.00 \times 10^{-3} (\pm 1.8 \times 10^{-12})$	$3.00 \times 10^{-5} (\pm 1.8 \times 10^{-12})$	$10.0 \times 10^3 (\pm 1.21 \times 10^{-3})$
11.5	$N(\xi = 000)$	$9.20 \times 10^{-7} (\pm 1.21 \times 10^{-6})$	$3.07 \times 10^{-5} (\pm 1.21 \times 10^{-6})$	$9.92 \times 10^3 (\pm 0.81 \times 10^3)$
11.5	$N(\xi = 100)$	$1.25 \times 10^{-6} (\pm 1.24 \times 10^{-6})$	$3.11 \times 10^{-5} (\pm 1.24 \times 10^{-6})$	$9.95 \times 10^3 (\pm 0.82 \times 10^3)$
11.5	$N(\xi = 200)$	$2.33 \times 10^{-6} (\pm 1.20 \times 10^{-6})$	$3.23 \times 10^{-5} (\pm 1.20 \times 10^{-6})$	$9.99 \times 10^3 (\pm 0.80 \times 10^3)$
11.5	$N(\xi = 300)$	$-1.30 \times 10^{-7} (\pm 1.21 \times 10^{-6})$	$2.97 \times 10^{-5} (\pm 1.21 \times 10^{-6})$	$9.90 \times 10^3 (\pm 0.81 \times 10^3)$
11.5	$N(\xi = 400)$	$-2.90 \times 10^{-7} (\pm 1.18 \times 10^{-6})$	$2.98 \times 10^{-5} (\pm 1.18 \times 10^{-6})$	$9.93 \times 10^3 (\pm 0.78 \times 10^3)$
11.5	$N(\xi = 500)$	$2.99 \times 10^{-6} (\pm 1.20 \times 10^{-6})$	$3.32 \times 10^{-5} (\pm 1.20 \times 10^{-6})$	$10.0 \times 10^3 (\pm 0.80 \times 10^3)$
11.5	$N(\xi = 600)$	$-1.20 \times 10^{-6} (\pm 1.28 \times 10^{-6})$	$2.88 \times 10^{-5} (\pm 1.28 \times 10^{-6})$	$10.0 \times 10^3 (\pm 0.85 \times 10^3)$
2.8	$N(\xi = 000)$	$3.83 \times 10^{-6} (\pm 5.28 \times 10^{-6})$	$3.29 \times 10^{-5} (\pm 5.29 \times 10^{-6})$	$9.69 \times 10^3 (\pm 3.52 \times 10^3)$
2.8	$N(\xi = 100)$	$5.62 \times 10^{-6} (\pm 5.49 \times 10^{-6})$	$3.51 \times 10^{-5} (\pm 5.47 \times 10^{-6})$	$9.82 \times 10^3 (\pm 3.65 \times 10^3)$
2.8	$N(\xi = 200)$	$1.05 \times 10^{-5} (\pm 5.40 \times 10^{-6})$	$4.05 \times 10^{-5} (\pm 5.36 \times 10^{-6})$	$10.0 \times 10^3 (\pm 3.59 \times 10^3)$
2.8	$N(\xi = 300)$	$-5.70 \times 10^{-7} (\pm 5.28 \times 10^{-6})$	$2.85 \times 10^{-5} (\pm 5.29 \times 10^{-6})$	$9.69 \times 10^3 (\pm 3.52 \times 10^3)$
2.8	$N(\xi = 400)$	$-1.33 \times 10^{-6} (\pm 5.32 \times 10^{-6})$	$2.89 \times 10^{-5} (\pm 5.32 \times 10^{-6})$	$10.0 \times 10^3 (\pm 3.55 \times 10^3)$
2.8	$N(\xi = 500)$	$1.36 \times 10^{-5} (\pm 5.53 \times 10^{-6})$	$4.45 \times 10^{-5} (\pm 5.48 \times 10^{-6})$	$10.3 \times 10^3 (\pm 3.66 \times 10^3)$
2.8	$N(\xi = 600)$	$-3.5 \times 10^{-6} (\pm 5.40 \times 10^{-6})$	$2.65 \times 10^{-5} (\pm 5.41 \times 10^{-6})$	$10.0 \times 10^3 (\pm 3.60 \times 10^3)$
-6.6	$N(\xi = 000)$	$7.63 \times 10^{-6} (\pm 1.13 \times 10^{-5})$	$3.57 \times 10^{-5} (\pm 1.14 \times 10^{-5})$	$9.35 \times 10^3 (\pm 7.53 \times 10^3)$
-6.6	$N(\xi = 100)$	$1.26 \times 10^{-5} (\pm 1.20 \times 10^{-5})$	$4.13 \times 10^{-5} (\pm 1.18 \times 10^{-5})$	$9.56 \times 10^3 (\pm 7.93 \times 10^3)$
-6.6	$N(\xi = 200)$	$2.38 \times 10^{-5} (\pm 1.21 \times 10^{-5})$	$5.37 \times 10^{-5} (\pm 1.19 \times 10^{-5})$	$9.96 \times 10^3 (\pm 7.93 \times 10^3)$
-6.6	$N(\xi = 300)$	$-1.23 \times 10^{-6} (\pm 1.14 \times 10^{-5})$	$2.69 \times 10^{-5} (\pm 1.14 \times 10^{-6})$	$9.37 \times 10^3 (\pm 7.60 \times 10^3)$
-6.6	$N(\xi = 400)$	$-3.21 \times 10^{-6} (\pm 1.20 \times 10^{-5})$	$2.74 \times 10^{-5} (\pm 1.19 \times 10^{-5})$	$10.2 \times 10^3 (\pm 7.93 \times 10^3)$
-6.6	$N(\xi = 500)$	$1.2577 \times 10^{-3} (\pm 7.91 \times 10^{-5})$	$1.2682 \times 10^{-3} (\pm 7.96 \times 10^{-5})$	$0.35 \times 10^3 (\pm 52.6 \times 10^3)^1$
-6.6	$N(\xi = 600)$	$-7.9 \times 10^{-6} (\pm 1.20 \times 10^{-5})$	$2.22 \times 10^{-5} (\pm 1.21 \times 10^{-5})$	$10.0 \times 10^3 (\pm 8.00 \times 10^3)$
-13.2	$N(\xi = 000)$	$1.23 \times 10^{-5} (\pm 2.12 \times 10^{-5})$	$3.87 \times 10^{-5} (\pm 2.14 \times 10^{-5})$	$8.80 \times 10^3 (\pm 14.2 \times 10^3)^1$
-13.2	$N(\xi = 100)$	$2.52 \times 10^{-5} (\pm 2.28 \times 10^{-5})$	$5.22 \times 10^{-5} (\pm 2.23 \times 10^{-5})$	$9.82 \times 10^3 (\pm 15.1 \times 10^3)^1$
-13.2	$N(\xi = 200)$	$7.61 \times 10^{-4} (\pm 3.93 \times 10^{-5})$	$7.64 \times 10^{-4} (\pm 3.98 \times 10^{-5})$	$0.12 \times 10^3 (\pm 26.4 \times 10^3)^1$
-13.2	$N(\xi = 300)$	$-2.40 \times 10^{-6} (\pm 2.14 \times 10^{-5})$	$2.41 \times 10^{-5} (\pm 2.15 \times 10^{-5})$	$8.83 \times 10^3 (\pm 14.3 \times 10^3)^1$
-13.2	$N(\xi = 400)$	$-6.60 \times 10^{-6} (\pm 2.42 \times 10^{-5})$	$2.41 \times 10^{-5} (\pm 2.42 \times 10^{-5})$	$10.2 \times 10^3 (\pm 16.1 \times 10^3)^1$
-13.2	$N(\xi = 500)$	$1.4261 \times 10^{-3} (\pm 30.0 \times 10^{-5})$	$1.4259 \times 10^{-3} (\pm 29.2 \times 10^{-5})$	$-0.06 \times 10^3 (\pm 190 \times 10^3)^1$
-13.2	$N(\xi = 600)$	$-1.0995 \times 10^{-3} (\pm 3.75 \times 10^{-5})$	$-1.0961 \times 10^{-3} (\pm 3.89 \times 10^{-5})$	$1.13 \times 10^3 (\pm 25.4 \times 10^3)^1$

¹Measurement is invalid.

TABLE III. Parameters and some characteristic numerical results of the measuring time shift $\tau = 3.0 \times 10^{-9}$ under Gaussian noise with different SNRs in the AWVA scheme. Here $1/T$ (units of MHz) represents the sampling frequency of the APD.

SNR*	$1/T$	$N(t, \xi_1)$	$N(t, \xi_2)$	Θ_0	Θ_τ	$\Delta\Theta$	K_2^M	$\bar{K}_2(\pm E_2)$
		no noise	no noise	1.2442×10^{-9}	1.1666×10^{-9}	7.76×10^{-11}	0.0258	
7.2	1	$\xi_1 = 000$	$\xi_2 = 700$	1.2462×10^{-9}	1.1678×10^{-9}	7.84×10^{-11}	0.0261	0.02590(± 0.0007)
7.2	1	$\xi_1 = 100$	$\xi_2 = 710$	1.2427×10^{-9}	1.1657×10^{-9}	7.70×10^{-11}	0.0256	0.02590(± 0.0007)
7.2	1	$\xi_1 = 200$	$\xi_2 = 720$	1.2452×10^{-9}	1.1654×10^{-9}	7.98×10^{-11}	0.0266	0.02590(± 0.0007)
7.2	1	$\xi_1 = 300$	$\xi_2 = 730$	1.2440×10^{-9}	1.1674×10^{-9}	7.66×10^{-11}	0.0255	0.02590(± 0.0007)
7.2	1	$\xi_1 = 400$	$\xi_2 = 740$	1.2454×10^{-9}	1.1680×10^{-9}	7.74×10^{-11}	0.0258	0.02590(± 0.0007)
7.2	1	$\xi_1 = 500$	$\xi_2 = 750$	1.2322×10^{-9}	1.1545×10^{-9}	7.77×10^{-11}	0.0259	0.02590(± 0.0007)
7.2	1	$\xi_1 = 600$	$\xi_2 = 770$	1.2591×10^{-9}	1.1817×10^{-9}	7.74×10^{-11}	0.0258	0.02590(± 0.0007)
-3.0	1	$\xi_1 = 000$	$\xi_2 = 700$	1.1508×10^{-9}	1.0698×10^{-9}	8.10×10^{-11}	0.0270	0.02595(± 0.0030)
-3.0	1	$\xi_1 = 100$	$\xi_2 = 710$	1.3055×10^{-9}	1.2308×10^{-9}	7.47×10^{-11}	0.0249	0.02595(± 0.0030)
-3.0	1	$\xi_1 = 200$	$\xi_2 = 720$	1.1987×10^{-9}	1.1117×10^{-9}	8.70×10^{-11}	0.0290	0.02595(± 0.0030)
-3.0	1	$\xi_1 = 300$	$\xi_2 = 730$	1.2190×10^{-9}	1.1465×10^{-9}	7.25×10^{-11}	0.0241	0.02595(± 0.0030)
-3.0	1	$\xi_1 = 400$	$\xi_2 = 740$	1.2657×10^{-9}	1.1893×10^{-9}	7.64×10^{-11}	0.0254	0.02595(± 0.0030)
-3.0	1	$\xi_1 = 500$	$\xi_2 = 750$	1.1748×10^{-9}	1.0971×10^{-9}	7.77×10^{-11}	0.0259	0.02595(± 0.0030)
-3.0	1	$\xi_1 = 600$	$\xi_2 = 770$	1.3835×10^{-9}	1.3072×10^{-9}	7.63×10^{-11}	0.0254	0.02595(± 0.0030)
-12.6	1	$\xi_1 = 000$	$\xi_2 = 700$	0.6719×10^{-9}	0.5867×10^{-9}	8.52×10^{-11}	0.0284	0.02608(± 0.0067)
-12.6	1	$\xi_1 = 100$	$\xi_2 = 710$	1.6234×10^{-9}	1.5524×10^{-9}	7.10×10^{-11}	0.0236	0.02608(± 0.0067)
-12.6	1	$\xi_1 = 200$	$\xi_2 = 720$	0.9655×10^{-9}	0.8671×10^{-9}	9.84×10^{-11}	0.0328	0.02608(± 0.0067)
-12.6	1	$\xi_1 = 300$	$\xi_2 = 730$	1.1025×10^{-9}	1.0363×10^{-9}	6.62×10^{-11}	0.0220	0.02608(± 0.0067)
-12.6	1	$\xi_1 = 400$	$\xi_2 = 740$	1.3512×10^{-9}	1.2762×10^{-9}	7.50×10^{-11}	0.0250	0.02608(± 0.0067)
-12.6	1	$\xi_1 = 500$	$\xi_2 = 750$	1.0343×10^{-9}	0.9565×10^{-9}	7.78×10^{-11}	0.0259	0.02608(± 0.0067)
-12.6	1	$\xi_1 = 600$	$\xi_2 = 770$	1.8158×10^{-9}	1.7411×10^{-9}	7.47×10^{-11}	0.0249	0.02608(± 0.0067)
-18.6	1	$\xi_1 = 000$	$\xi_2 = 700$	1.3079×10^{-9}	1.2151×10^{-9}	9.28×10^{-11}	0.0309	0.02264(± 0.0085)
-18.6	1	$\xi_1 = 100$	$\xi_2 = 710$	2.8789×10^{-9}	2.8145×10^{-9}	6.44×10^{-11}	0.0214	0.02264(± 0.0085)
-18.6	1	$\xi_1 = 200$	$\xi_2 = 720$	0.4317×10^{-9}	0.3892×10^{-9}	4.25×10^{-11}	0.0141	0.02264(± 0.0085)
-18.6	1	$\xi_1 = 300$	$\xi_2 = 730$	0.6522×10^{-9}	0.5974×10^{-9}	5.48×10^{-11}	0.0182	0.02264(± 0.0085)
-18.6	1	$\xi_1 = 400$	$\xi_2 = 740$	1.6710×10^{-9}	1.5987×10^{-9}	7.23×10^{-11}	0.0241	0.02264(± 0.0085)
-18.6	1	$\xi_1 = 500$	$\xi_2 = 750$	0.6262×10^{-9}	0.5484×10^{-9}	7.78×10^{-11}	0.0259	0.02264(± 0.0085)
-18.6	1	$\xi_1 = 600$	$\xi_2 = 770$	3.3287×10^{-9}	3.2569×10^{-9}	7.18×10^{-11}	0.0239	0.02264(± 0.0085)
-18.6	10	$\xi_1 = 000$	$\xi_2 = 700$	1.5115×10^{-9}	1.4299×10^{-9}	8.16×10^{-11}	0.0272	0.02551(± 0.0028)
-18.6	10	$\xi_1 = 100$	$\xi_2 = 710$	2.2062×10^{-9}	2.1381×10^{-9}	6.81×10^{-11}	0.0227	0.02551(± 0.0028)
-18.6	10	$\xi_1 = 200$	$\xi_2 = 720$	0.8213×10^{-9}	0.7503×10^{-9}	7.10×10^{-11}	0.0236	0.02551(± 0.0028)
-18.6	10	$\xi_1 = 300$	$\xi_2 = 730$	1.5151×10^{-9}	1.4387×10^{-9}	7.64×10^{-11}	0.0254	0.02551(± 0.0028)
-18.6	10	$\xi_1 = 400$	$\xi_2 = 740$	1.8597×10^{-9}	1.7841×10^{-9}	7.56×10^{-11}	0.0252	0.02551(± 0.0028)
-18.6	10	$\xi_1 = 500$	$\xi_2 = 750$	1.2757×10^{-9}	1.1975×10^{-9}	7.82×10^{-11}	0.0260	0.02551(± 0.0028)
-18.6	10	$\xi_1 = 600$	$\xi_2 = 770$	1.8199×10^{-9}	1.7344×10^{-9}	8.55×10^{-11}	0.0285	0.02551(± 0.0028)
-18.6	100	$\xi_1 = 000$	$\xi_2 = 700$	1.2195×10^{-9}	1.1449×10^{-9}	7.46×10^{-11}	0.0248	0.02568(± 0.0008)
-18.6	100	$\xi_1 = 100$	$\xi_2 = 710$	1.5641×10^{-9}	1.4852×10^{-9}	7.89×10^{-11}	0.0263	0.02568(± 0.0008)
-18.6	100	$\xi_1 = 200$	$\xi_2 = 720$	0.9090×10^{-9}	0.8319×10^{-9}	7.71×10^{-11}	0.0257	0.02568(± 0.0008)
-18.6	100	$\xi_1 = 300$	$\xi_2 = 730$	1.2707×10^{-9}	1.1929×10^{-9}	7.78×10^{-11}	0.0259	0.02568(± 0.0008)
-18.6	100	$\xi_1 = 400$	$\xi_2 = 740$	1.2711×10^{-9}	1.1931×10^{-9}	7.80×10^{-11}	0.0260	0.02568(± 0.0008)
-18.6	100	$\xi_1 = 500$	$\xi_2 = 750$	1.2311×10^{-9}	1.1559×10^{-9}	7.52×10^{-11}	0.0250	0.02568(± 0.0008)
-18.6	100	$\xi_1 = 600$	$\xi_2 = 770$	1.4695×10^{-9}	1.3910×10^{-9}	7.85×10^{-11}	0.0261	0.02568(± 0.0008)

TABLE IV. Numerical results (dimensional quantities in unit of s) for measuring the different τ under the strong noise at SNR equal to -13.2 dB in the WVA scheme. The contents E_{t_0} and E_{t_τ} in parentheses represent the standard error for estimating the time shifts δt_0 and δt_τ , respectively. Here $\mathbf{N}(\xi = 0)$, $\mathbf{N}(\xi = 100)$, \dots , $\mathbf{N}(\xi = 600)$ represent the multiple measurements with the different initial times.

τ	Noise	$\delta t_0(\pm E_{t_0})$	$\delta t_\tau(\pm E_{t_\tau})$	$K_1(\pm E_1)$
6×10^{-9}	$N(\xi = 000)$	$1.23 \times 10^{-5} (\pm 2.12 \times 10^{-5})$	$6.57 \times 10^{-5} (\pm 2.16 \times 10^{-5})$	$8.90 \times 10^3 (\pm 7.13 \times 10^3)$
6×10^{-9}	$N(\xi = 100)$	$2.52 \times 10^{-5} (\pm 2.28 \times 10^{-5})$	$7.85 \times 10^{-5} (\pm 2.20 \times 10^{-5})$	$8.88 \times 10^3 (\pm 7.46 \times 10^3)$
6×10^{-9}	$N(\xi = 200)$	$7.6086 \times 10^{-4} (\pm 3.93 \times 10^{-5})$	$7.7576 \times 10^{-4} (\pm 4.28 \times 10^{-5})$	$2.48 \times 10^3 (\pm 13.6 \times 10^3)^1$
6×10^{-9}	$N(\xi = 300)$	$-2.40 \times 10^{-6} (\pm 2.14 \times 10^{-5})$	$5.07 \times 10^{-5} (\pm 2.15 \times 10^{-5})$	$8.85 \times 10^3 (\pm 7.15 \times 10^3)$
6×10^{-9}	$N(\xi = 400)$	$-6.60 \times 10^{-6} (\pm 2.42 \times 10^{-5})$	$5.49 \times 10^{-5} (\pm 2.41 \times 10^{-5})$	$10.2 \times 10^3 (\pm 8.05 \times 10^3)$
6×10^{-9}	$N(\xi = 500)$	$1.4261 \times 10^{-3} (\pm 30.0 \times 10^{-5})$	$1.4251 \times 10^{-3} (\pm 28.2 \times 10^{-5})$	$-0.16 \times 10^3 (\pm 98.6 \times 10^3)^1$
6×10^{-9}	$N(\xi = 600)$	$-1.0995 \times 10^{-3} (\pm 3.75 \times 10^{-5})$	$-1.0920 \times 10^{-3} (\pm 4.07 \times 10^{-5})$	$1.25 \times 10^3 (\pm 13.0 \times 10^3)^1$
9×10^{-9}	$N(\xi = 000)$	$1.23 \times 10^{-5} (\pm 2.12 \times 10^{-5})$	$9.34 \times 10^{-5} (\pm 2.19 \times 10^{-5})$	$9.01 \times 10^3 (\pm 4.84 \times 10^3)$
9×10^{-9}	$N(\xi = 100)$	$2.52 \times 10^{-5} (\pm 2.28 \times 10^{-5})$	$10.4 \times 10^{-5} (\pm 2.18 \times 10^{-5})$	$8.75 \times 10^3 (\pm 5.22 \times 10^3)$
9×10^{-9}	$N(\xi = 200)$	$7.6086 \times 10^{-4} (\pm 3.93 \times 10^{-5})$	$7.8843 \times 10^{-4} (\pm 4.58 \times 10^{-5})$	$3.05 \times 10^3 (\pm 9.45 \times 10^3)^1$
9×10^{-9}	$N(\xi = 300)$	$-2.40 \times 10^{-6} (\pm 2.14 \times 10^{-5})$	$7.72 \times 10^{-5} (\pm 2.16 \times 10^{-5})$	$8.84 \times 10^3 (\pm 4.77 \times 10^3)$
9×10^{-9}	$N(\xi = 400)$	$-6.60 \times 10^{-6} (\pm 2.42 \times 10^{-5})$	$8.58 \times 10^{-5} (\pm 2.39 \times 10^{-5})$	$10.3 \times 10^3 (\pm 5.34 \times 10^3)$
9×10^{-9}	$N(\xi = 500)$	$1.4261 \times 10^{-3} (\pm 30.0 \times 10^{-5})$	$1.4238 \times 10^{-3} (\pm 26.8 \times 10^{-5})$	$-0.25 \times 10^3 (\pm 65.5 \times 10^3)^1$
9×10^{-9}	$N(\xi = 600)$	$-1.0995 \times 10^{-3} (\pm 3.75 \times 10^{-5})$	$-1.0869 \times 10^{-3} (\pm 4.31 \times 10^{-5})$	$1.38 \times 10^3 (\pm 8.95 \times 10^3)^1$
12×10^{-9}	$N(\xi = 000)$	$1.23 \times 10^{-5} (\pm 2.12 \times 10^{-5})$	$12.2 \times 10^{-5} (\pm 2.23 \times 10^{-5})$	$9.12 \times 10^3 (\pm 3.62 \times 10^3)$
12×10^{-9}	$N(\xi = 100)$	$2.52 \times 10^{-5} (\pm 2.28 \times 10^{-5})$	$13.1 \times 10^{-5} (\pm 2.18 \times 10^{-5})$	$8.77 \times 10^3 (\pm 3.75 \times 10^3)$
12×10^{-9}	$N(\xi = 200)$	$7.6086 \times 10^{-4} (\pm 3.93 \times 10^{-5})$	$8.1703 \times 10^{-4} (\pm 5.26 \times 10^{-5})$	$4.68 \times 10^3 (\pm 7.65 \times 10^3)^1$
12×10^{-9}	$N(\xi = 300)$	$-2.40 \times 10^{-6} (\pm 2.14 \times 10^{-5})$	$10.4 \times 10^{-5} (\pm 2.16 \times 10^{-5})$	$9.21 \times 10^3 (\pm 2.68 \times 10^3)$
12×10^{-9}	$N(\xi = 400)$	$-6.60 \times 10^{-6} (\pm 2.42 \times 10^{-5})$	$11.7 \times 10^{-5} (\pm 2.37 \times 10^{-5})$	$10.3 \times 10^3 (\pm 3.99 \times 10^3)$
12×10^{-9}	$N(\xi = 500)$	$1.4261 \times 10^{-3} (\pm 30.0 \times 10^{-5})$	$1.4217 \times 10^{-3} (\pm 25.2 \times 10^{-5})$	$-0.36 \times 10^3 (\pm 45.8 \times 10^3)^1$
12×10^{-9}	$N(\xi = 600)$	$-1.0995 \times 10^{-3} (\pm 4.66 \times 10^{-5})$	$-1.0797 \times 10^{-3} (\pm 4.63 \times 10^{-5})$	$1.65 \times 10^3 (\pm 7.40 \times 10^3)^1$
15×10^{-9}	$N(\xi = 000)$	$1.23 \times 10^{-5} (\pm 2.12 \times 10^{-5})$	$15.7 \times 10^{-5} (\pm 2.27 \times 10^{-5})$	$9.23 \times 10^3 (\pm 2.92 \times 10^3)$
15×10^{-9}	$N(\xi = 100)$	$2.52 \times 10^{-5} (\pm 2.28 \times 10^{-5})$	$15.6 \times 10^{-5} (\pm 2.18 \times 10^{-5})$	$8.76 \times 10^3 (\pm 2.96 \times 10^3)$
15×10^{-9}	$N(\xi = 200)$	$7.6086 \times 10^{-4} (\pm 3.93 \times 10^{-5})$	$8.6756 \times 10^{-4} (\pm 6.45 \times 10^{-5})$	$7.11 \times 10^3 (\pm 6.92 \times 10^3)$
15×10^{-9}	$N(\xi = 300)$	$-2.40 \times 10^{-6} (\pm 2.14 \times 10^{-5})$	$13.1 \times 10^{-5} (\pm 2.16 \times 10^{-5})$	$8.86 \times 10^3 (\pm 2.86 \times 10^3)$
15×10^{-9}	$N(\xi = 400)$	$-6.60 \times 10^{-6} (\pm 2.42 \times 10^{-5})$	$14.7 \times 10^{-5} (\pm 2.34 \times 10^{-5})$	$10.3 \times 10^3 (\pm 3.17 \times 10^3)$
15×10^{-9}	$N(\xi = 500)$	$1.4261 \times 10^{-3} (\pm 30.0 \times 10^{-5})$	$1.4187 \times 10^{-3} (\pm 24.0 \times 10^{-5})$	$-0.49 \times 10^3 (\pm 36.0 \times 10^3)^1$
15×10^{-9}	$N(\xi = 600)$	$-1.0995 \times 10^{-3} (\pm 3.75 \times 10^{-5})$	$-1.0687 \times 10^{-3} (\pm 5.24 \times 10^{-5})$	$2.05 \times 10^3 (\pm 5.99 \times 10^3)^1$

¹Measurement is invalid.

TABLE V. Parameters and some characteristic numerical results for measuring the different τ under the strong noises $\mathbf{N}(t, \sigma^2, \xi_1)$ and $\mathbf{N}(t, \sigma^2, \xi_2)$ at SNR* equal to -18.6 dB in the AWVA scheme. The sampling frequency is set at $1/T = 10$ MHz.

τ (s)	$\mathbf{N}(t, \xi_1)$	$\mathbf{N}(t, \xi_2)$	Θ_0	Θ_τ	$\Delta\Theta$	K_2^M	$\bar{K}_2(\pm E_2)$
	no noise	no noise	1.2443×10^{-9}	1.0837×10^{-9}	16.1×10^{-11}	0.0268	
6×10^{-9}	$N(\xi_1 = 000)$	$N(\xi_2 = 700)$	1.5116×10^{-9}	1.3418×10^{-9}	17.0×10^{-11}	0.0283	0.02643(± 0.00287)
6×10^{-9}	$N(\xi_1 = 100)$	$N(\xi_2 = 710)$	2.2062×10^{-9}	2.0626×10^{-9}	14.3×10^{-11}	0.0238	0.02643(± 0.00287)
6×10^{-9}	$N(\xi_1 = 200)$	$N(\xi_2 = 720)$	0.8214×10^{-9}	0.6742×10^{-9}	14.7×10^{-11}	0.0245	0.02643(± 0.00287)
6×10^{-9}	$N(\xi_1 = 300)$	$N(\xi_2 = 730)$	1.5151×10^{-9}	1.3575×10^{-9}	15.7×10^{-11}	0.0261	0.02643(± 0.00287)
6×10^{-9}	$N(\xi_1 = 400)$	$N(\xi_2 = 740)$	1.8597×10^{-9}	1.7035×10^{-9}	15.6×10^{-11}	0.0260	0.02643(± 0.00287)
6×10^{-9}	$N(\xi_1 = 500)$	$N(\xi_2 = 750)$	1.2757×10^{-9}	1.1136×10^{-9}	16.2×10^{-11}	0.0270	0.02643(± 0.00287)
6×10^{-9}	$N(\xi_1 = 600)$	$N(\xi_2 = 760)$	1.8199×10^{-9}	1.6441×10^{-9}	17.6×10^{-11}	0.0293	0.02643(± 0.00287)
	no noise	no noise	1.2443×10^{-9}	0.9973×10^{-9}	24.7×10^{-11}	0.0274	
9×10^{-9}	$N(\xi_1 = 000)$	$N(\xi_2 = 700)$	1.5116×10^{-9}	1.2490×10^{-9}	26.2×10^{-11}	0.0291	0.02720(± 0.00280)
9×10^{-9}	$N(\xi_1 = 100)$	$N(\xi_2 = 710)$	2.2062×10^{-9}	1.9815×10^{-9}	22.4×10^{-11}	0.0249	0.02720(± 0.00280)
9×10^{-9}	$N(\xi_1 = 200)$	$N(\xi_2 = 720)$	0.8214×10^{-9}	0.5944×10^{-9}	22.7×10^{-11}	0.0252	0.02720(± 0.00280)
9×10^{-9}	$N(\xi_1 = 300)$	$N(\xi_2 = 730)$	1.5151×10^{-9}	1.2730×10^{-9}	24.2×10^{-11}	0.0269	0.02720(± 0.00280)
9×10^{-9}	$N(\xi_1 = 400)$	$N(\xi_2 = 740)$	1.8597×10^{-9}	1.6194×10^{-9}	24.0×10^{-11}	0.0266	0.02720(± 0.00280)
9×10^{-9}	$N(\xi_1 = 500)$	$N(\xi_2 = 750)$	1.2757×10^{-9}	1.0260×10^{-9}	25.0×10^{-11}	0.0277	0.02720(± 0.00280)
9×10^{-9}	$N(\xi_1 = 600)$	$N(\xi_2 = 760)$	1.8199×10^{-9}	1.5501×10^{-9}	27.0×10^{-11}	0.0300	0.02720(± 0.00280)
	no noise	no noise	1.2443×10^{-9}	0.9091×10^{-9}	33.5×10^{-11}	0.0279	
12×10^{-9}	$N(\xi_1 = 000)$	$N(\xi_2 = 700)$	1.5116×10^{-9}	1.1535×10^{-9}	35.8×10^{-11}	0.0298	0.02770(± 0.00250)
12×10^{-9}	$N(\xi_1 = 100)$	$N(\xi_2 = 710)$	2.2062×10^{-9}	1.8966×10^{-9}	30.9×10^{-11}	0.0257	0.02770(± 0.00250)
12×10^{-9}	$N(\xi_1 = 200)$	$N(\xi_2 = 720)$	0.8214×10^{-9}	0.5128×10^{-9}	30.8×10^{-11}	0.0256	0.02770(± 0.00250)
12×10^{-9}	$N(\xi_1 = 300)$	$N(\xi_2 = 730)$	1.5151×10^{-9}	1.1870×10^{-9}	32.8×10^{-11}	0.0273	0.02770(± 0.00250)
12×10^{-9}	$N(\xi_1 = 400)$	$N(\xi_2 = 740)$	1.8597×10^{-9}	1.5336×10^{-9}	32.6×10^{-11}	0.0271	0.02770(± 0.00250)
12×10^{-9}	$N(\xi_1 = 500)$	$N(\xi_2 = 750)$	1.2757×10^{-9}	0.9364×10^{-9}	33.9×10^{-11}	0.0282	0.02770(± 0.00250)
12×10^{-9}	$N(\xi_1 = 600)$	$N(\xi_2 = 760)$	1.8199×10^{-9}	1.4566×10^{-9}	36.3×10^{-11}	0.0302	0.02770(± 0.00250)
	no noise	no noise	1.2443×10^{-9}	0.8208×10^{-9}	43.4×10^{-11}	0.0282	
15×10^{-9}	$N(\xi_1 = 000)$	$N(\xi_2 = 700)$	1.5116×10^{-9}	1.0575×10^{-9}	45.4×10^{-11}	0.0303	0.02811(± 0.00229)
15×10^{-9}	$N(\xi_1 = 100)$	$N(\xi_2 = 710)$	2.2062×10^{-9}	1.8100×10^{-9}	39.6×10^{-11}	0.0264	0.02811(± 0.00229)
15×10^{-9}	$N(\xi_1 = 200)$	$N(\xi_2 = 720)$	0.8214×10^{-9}	0.4308×10^{-9}	39.1×10^{-11}	0.0261	0.02811(± 0.00229)
15×10^{-9}	$N(\xi_1 = 300)$	$N(\xi_2 = 730)$	1.5151×10^{-9}	1.1010×10^{-9}	41.4×10^{-11}	0.0276	0.02811(± 0.00229)
15×10^{-9}	$N(\xi_1 = 400)$	$N(\xi_2 = 740)$	1.8597×10^{-9}	1.4477×10^{-9}	41.2×10^{-11}	0.0274	0.02811(± 0.00229)
15×10^{-9}	$N(\xi_1 = 500)$	$N(\xi_2 = 750)$	1.2757×10^{-9}	0.8466×10^{-9}	42.9×10^{-11}	0.0286	0.02811(± 0.00229)
15×10^{-9}	$N(\xi_1 = 600)$	$N(\xi_2 = 760)$	1.8199×10^{-9}	1.3628×10^{-9}	45.7×10^{-11}	0.0304	0.02811(± 0.00229)

TABLE VI. Parameters and some characteristic numerical results for measuring the different τ under the strong noises $\mathbf{N}(t, \sigma^2, \xi_1)$ and $\mathbf{N}(t, \sigma^2, \xi_2)$ at SNR* equal to -18.6 dB in the AWVA scheme. The sampling frequency is set at $1/T = 100$ MHz.

τ (s)	$\mathbf{N}(t, \xi_1)$	$\mathbf{N}(t, \xi_2)$	Θ_0	Θ_τ	$\Delta\Theta$	K_2^M	$\bar{K}_2(\pm E_2)$
6×10^{-9}	no noise	no noise	1.2443×10^{-9}	1.0837×10^{-9}	16.1×10^{-11}	0.0267	
6×10^{-9}	$N(\xi_1 = 000)$	$N(\xi_2 = 700)$	1.2195×10^{-9}	1.0651×10^{-9}	15.4×10^{-11}	0.0257	0.02654(± 0.00084)
6×10^{-9}	$N(\xi_1 = 100)$	$N(\xi_2 = 710)$	1.5641×10^{-9}	1.4010×10^{-9}	16.3×10^{-11}	0.0272	0.02654(± 0.00084)
6×10^{-9}	$N(\xi_1 = 200)$	$N(\xi_2 = 720)$	0.9090×10^{-9}	0.7495×10^{-9}	15.9×10^{-11}	0.0265	0.02654(± 0.00084)
6×10^{-9}	$N(\xi_1 = 300)$	$N(\xi_2 = 730)$	1.2707×10^{-9}	1.1104×10^{-9}	16.0×10^{-11}	0.0266	0.02654(± 0.00084)
6×10^{-9}	$N(\xi_1 = 400)$	$N(\xi_2 = 740)$	1.2711×10^{-9}	1.1095×10^{-9}	16.1×10^{-11}	0.0268	0.02654(± 0.00084)
6×10^{-9}	$N(\xi_1 = 500)$	$N(\xi_2 = 750)$	1.2311×10^{-9}	1.0754×10^{-9}	15.6×10^{-11}	0.0260	0.02654(± 0.00084)
6×10^{-9}	$N(\xi_1 = 600)$	$N(\xi_2 = 760)$	1.4695×10^{-9}	1.3071×10^{-9}	16.2×10^{-11}	0.0270	0.02654(± 0.00084)
	no noise	no noise	1.2443×10^{-9}	0.9973×10^{-9}	24.7×10^{-11}	0.0274	
9×10^{-9}	$N(\xi_1 = 000)$	$N(\xi_2 = 700)$	1.2195×10^{-9}	0.9818×10^{-9}	23.8×10^{-11}	0.0264	0.02727(± 0.00087)
9×10^{-9}	$N(\xi_1 = 100)$	$N(\xi_2 = 710)$	1.5641×10^{-9}	1.3132×10^{-9}	25.1×10^{-11}	0.0279	0.02727(± 0.00087)
9×10^{-9}	$N(\xi_1 = 200)$	$N(\xi_2 = 720)$	0.9090×10^{-9}	0.6636×10^{-9}	24.5×10^{-11}	0.0272	0.02727(± 0.00087)
9×10^{-9}	$N(\xi_1 = 300)$	$N(\xi_2 = 730)$	1.2707×10^{-9}	1.0246×10^{-9}	24.6×10^{-11}	0.0273	0.02727(± 0.00087)
9×10^{-9}	$N(\xi_1 = 400)$	$N(\xi_2 = 740)$	1.2711×10^{-9}	1.0223×10^{-9}	24.8×10^{-11}	0.0276	0.02727(± 0.00087)
9×10^{-9}	$N(\xi_1 = 500)$	$N(\xi_2 = 750)$	1.2311×10^{-9}	0.9914×10^{-9}	24.0×10^{-11}	0.0267	0.02727(± 0.00087)
9×10^{-9}	$N(\xi_1 = 600)$	$N(\xi_2 = 760)$	1.4695×10^{-9}	1.2196×10^{-9}	25.0×10^{-11}	0.0278	0.02727(± 0.00087)
	no noise	no noise	1.2443×10^{-9}	0.9091×10^{-9}	33.5×10^{-11}	0.0279	
12×10^{-9}	$N(\xi_1 = 000)$	$N(\xi_2 = 700)$	1.2195×10^{-9}	0.8967×10^{-9}	32.3×10^{-11}	0.0269	0.02774(± 0.00084)
12×10^{-9}	$N(\xi_1 = 100)$	$N(\xi_2 = 710)$	1.5641×10^{-9}	1.2236×10^{-9}	34.1×10^{-11}	0.0284	0.02774(± 0.00084)
12×10^{-9}	$N(\xi_1 = 200)$	$N(\xi_2 = 720)$	0.9090×10^{-9}	0.5760×10^{-9}	33.3×10^{-11}	0.0277	0.02774(± 0.00084)
12×10^{-9}	$N(\xi_1 = 300)$	$N(\xi_2 = 730)$	1.2707×10^{-9}	0.9375×10^{-9}	33.3×10^{-11}	0.0277	0.02774(± 0.00084)
12×10^{-9}	$N(\xi_1 = 400)$	$N(\xi_2 = 740)$	1.2711×10^{-9}	0.9332×10^{-9}	33.8×10^{-11}	0.0282	0.02774(± 0.00084)
12×10^{-9}	$N(\xi_1 = 500)$	$N(\xi_2 = 750)$	1.2311×10^{-9}	0.9056×10^{-9}	32.5×10^{-11}	0.0271	0.02774(± 0.00084)
12×10^{-9}	$N(\xi_1 = 600)$	$N(\xi_2 = 760)$	1.4695×10^{-9}	1.1301×10^{-9}	33.9×10^{-11}	0.0282	0.02774(± 0.00084)
	no noise	no noise	1.2443×10^{-9}	0.8208×10^{-9}	43.4×10^{-11}	0.0282	
15×10^{-9}	$N(\xi_1 = 000)$	$N(\xi_2 = 700)$	1.2195×10^{-9}	0.8115×10^{-9}	40.8×10^{-11}	0.0272	0.02808(± 0.00088)
15×10^{-9}	$N(\xi_1 = 100)$	$N(\xi_2 = 710)$	1.5641×10^{-9}	1.1339×10^{-9}	43.0×10^{-11}	0.0287	0.02808(± 0.00088)
15×10^{-9}	$N(\xi_1 = 200)$	$N(\xi_2 = 720)$	0.9090×10^{-9}	0.4883×10^{-9}	42.1×10^{-11}	0.0281	0.02808(± 0.00088)
15×10^{-9}	$N(\xi_1 = 300)$	$N(\xi_2 = 730)$	1.2707×10^{-9}	0.8505×10^{-9}	42.0×10^{-11}	0.0280	0.02808(± 0.00088)
15×10^{-9}	$N(\xi_1 = 400)$	$N(\xi_2 = 740)$	1.2711×10^{-9}	0.8438×10^{-9}	42.7×10^{-11}	0.0285	0.02808(± 0.00088)
15×10^{-9}	$N(\xi_1 = 500)$	$N(\xi_2 = 750)$	1.2311×10^{-9}	0.8195×10^{-9}	41.2×10^{-11}	0.0275	0.02808(± 0.00088)
15×10^{-9}	$N(\xi_1 = 600)$	$N(\xi_2 = 760)$	1.4695×10^{-9}	1.0405×10^{-9}	42.9×10^{-11}	0.0286	0.02808(± 0.00088)

- [1] Y. Aharonov, D. Z. Albert, and L. Vaidman, How the Result of a Measurement of a Component of the Spin of a Spin- $\frac{1}{2}$ Particle Can Turn Out to be 100, *Phys. Rev. Lett.* **60**, 1351 (1988).
- [2] J. Dressel, M. Malik, F. M. Miatto, A. N. Jordan, and R. W. Boyd, *Colloquium: Understanding quantum weak values: Basics and applications*, *Rev. Mod. Phys.* **86**, 307 (2014).
- [3] J. Ren, L. Qin, W. Feng, and X.-Q. Li, Weak-value-amplification analysis beyond the Aharonov-Albert-Vaidman Limit, *Phys. Rev. A* **102**, 042601 (2020).
- [4] P. Yin, W.-H. Zhang, L. Xu, Z.-G. Liu, W.-F. Zhuang, L. Chen, M. Gong, Y. Ma, X.-X. Peng, G.-C. Li, J.-S. Xu, Z.-Q. Zhou, L. Zhang, G. Chen, C.-F. Li, and G.-C. Guo, Improving the precision of optical metrology by detecting fewer photons with biased weak measurement, *Light Sci. Appl.* **10**, 103 (2021).
- [5] F. Lecocq, L. Ranzani, G. A. Peterson, K. Cicak, X. Y. Jin, R. W. Simmonds, J. D. Teufel, and J. Aumentado, Efficient Qubit Measurement with a Nonreciprocal Microwave Amplifier, *Phys. Rev. Lett.* **126**, 020502 (2021).
- [6] C. Krafczyk, A. N. Jordan, M. E. Goggin, and P. G. Kwiat, Enhanced Weak-Value Amplification via Photon Recycling, *Phys. Rev. Lett.* **126**, 220801 (2021).
- [7] J. S. Lundeen and C. Bamber, Procedure for Direct Measurement of General Quantum States Using Weak Measurement, *Phys. Rev. Lett.* **108**, 070402 (2012).

- [8] L. Xu, Z. Liu, A. Datta, G. C. Knee, J. S. Lundeen, Y.-q. Lu, and L. Zhang, Approaching Quantum-Limited Metrology with Imperfect Detectors by Using Weak-Value Amplification, *Phys. Rev. Lett.* **125**, 080501 (2020).
- [9] F.-Y. Ma, J.-G. Li, and J. Zou, The influence of non-Gaussian noise on weak values, *Phys. Lett. A* **388**, 127027 (2021).
- [10] N. Brunner and C. Simon, Measuring Small Longitudinal Phase Shifts: Weak Measurements or Standard Interferometry?, *Phys. Rev. Lett.* **105**, 010405 (2010).
- [11] G. I. Viza, J. Martínez-Rincón, G. A. Howland, H. Frostig, I. Shomroni, B. Dayan, and J. C. Howell, Weak-values technique for velocity measurements, *Opt. Lett.* **38**, 2949 (2013).
- [12] Z. Li, L. Xie, Q. Ti, P. Duan, Z. Zhang, and C. Ren, Increasing the dynamic range of weak measurement with two pointers, *Phys. Rev. A* **102**, 023701 (2020).
- [13] J.-H. Huang, F.-F. He, X.-Y. Duan, G.-J. Wang, and X.-Y. Hu, Modified weak-value-amplification technique for measuring a mirror's velocity based on the Vernier effect, *Phys. Rev. A* **105**, 013718 (2022).
- [14] P. B. Dixon, D. J. Starling, A. N. Jordan, and J. C. Howell, Ultrasensitive Beam Deflection Measurement via Interferometric Weak Value Amplification, *Phys. Rev. Lett.* **102**, 173601 (2009).
- [15] S. Kocsis, B. Braverman, S. Ravets, M. J. Stevens, R. P. Mirin, L. K. Shalm, and A. M. Steinberg, Observing the average trajectories of single photons in a two-slit interferometer, *Science* **332**, 1170 (2011).
- [16] X.-Y. Xu, Y. Kedem, K. Sun, L. Vaidman, C.-F. Li, and G.-C. Guo, Phase Estimation with Weak Measurement Using a White Light Source, *Phys. Rev. Lett.* **111**, 033604 (2013).
- [17] Y. Yang, Y. Xu, T. Guan, L. Shi, J. Li, D. Li, Y. He, X. Wang, Z. Li, and Y. Ji, Spectrum intensity ratio detection for frequency domain weak measurement system, *IEEE Photon. J.* **12**, 1 (2020).
- [18] B. de Lima Bernardo, S. Azevedo, and A. Rosas, Ultrasmall polarization rotation measurements via weak value amplification, *Phys. Lett. A* **378**, 2029 (2014).
- [19] O. S. Magaña-Loaiza, M. Mirhosseini, B. Rodenburg, and R. W. Boyd, Amplification of Angular Rotations Using Weak Measurements, *Phys. Rev. Lett.* **112**, 200401 (2014).
- [20] C. Ferrie and J. Combes, Weak Value Amplification is Suboptimal for Estimation and Detection, *Phys. Rev. Lett.* **112**, 040406 (2014).
- [21] G. C. Knee and E. M. Gauger, When Amplification with Weak Values Fails to Suppress Technical Noise, *Phys. Rev. X* **4**, 011032 (2014).
- [22] J. Zhu, Z. Li, Y. Liu, Y. Ye, Q. Ti, Z. Zhang, and F. Gao, Weak measurement with the peak-contrast-ratio pointer, *Phys. Rev. A* **103**, 032212 (2021).
- [23] D. Braun, P. Jian, O. Pinel, and N. Treps, Precision measurements with photon-subtracted or photon-added Gaussian states, *Phys. Rev. A* **90**, 013821 (2014).
- [24] S. M. H. Rafsanjani, M. Mirhosseini, O. S. M. na Loaiza, B. T. Gard, R. Birrittella, B. E. Koltenbah, C. G. Parazzoli, B. A. Capron, C. C. Gerry, J. P. Dowling, and R. W. Boyd, Quantum-enhanced interferometry with weak thermal light, *Optica* **4**, 487 (2017).
- [25] G. V. Avosopiants, B. I. Bantysh, K. G. Katamadze, N. A. Bogdanova, Y. I. Bogdanov, and S. P. Kulik, Statistical parameter estimation of multimode multiphoton-subtracted thermal states of light, *Phys. Rev. A* **104**, 013710 (2021).
- [26] H. Wu, P. Wu, Z.-C. Luo, L.-P. Xu, J.-H. Xie, T.-Y. Chang, H.-F. Shi, C.-L. Du, and H.-L. Cui, Pragmatic implementation of non-Gaussian devices of noise-limited weak value amplification, *IEEE Photon. J.* **13**, 1 (2021).
- [27] R. F. Fox, I. R. Gatland, R. Roy, and G. Vemuri, Fast, accurate algorithm for numerical simulation of exponentially correlated colored noise, *Phys. Rev. A* **38**, 5938 (1988).
- [28] B. L. Hu, J. P. Paz, and Y. Zhang, Quantum Brownian motion in a general environment: Exact master equation with nonlocal dissipation and colored noise, *Phys. Rev. D* **45**, 2843 (1992).
- [29] J.-L. Wu, W.-L. Duan, Y. Luo, and F. Yang, Time delay and non-Gaussian noise-enhanced stability of foraging colony system, *Physica A* **553**, 124253 (2020).
- [30] O. V. Pountounigni, R. Yamapi, C. Tchawoua, V. Pierro, and G. Filatrella, Detection of signals in presence of noise through Josephson junction switching currents, *Phys. Rev. E* **101**, 052205 (2020).
- [31] M. Parikh, F. Wilczek, and G. Zahariade, Signatures of the quantization of gravity at gravitational wave detectors, *Phys. Rev. D* **104**, 046021 (2021).
- [32] J. Tugnait, Time delay estimation with unknown spatially correlated gaussian noise, *IEEE Trans. Signal Process.* **41**, 549 (1993).
- [33] K. Wong, J. Wu, T. Davidson, Q. Jin, and P.-C. Ching, Performance of wavelet packet-division multiplexing in impulsive and gaussian noise, *IEEE Trans. Commun.* **48**, 1083 (2000).
- [34] X. Sun, M. Perc, Q. Lu, and J. Kurths, Effects of correlated gaussian noise on the mean firing rate and correlations of an electrically coupled neuronal network, *Chaos* **20**, 033116 (2010).
- [35] M. J. W. Hall, Gaussian noise and quantum-optical communication, *Phys. Rev. A* **50**, 3295 (1994).
- [36] T. C. Ralph, Quantum error correction of continuous-variable states against Gaussian noise, *Phys. Rev. A* **84**, 022339 (2011).
- [37] L. Bakmou and M. Daoud, Ultimate precision of joint parameter estimation under noisy Gaussian environment, *Phys. Lett. A* **428**, 127947 (2022).
- [38] A. Feizpour, X. Xing, and A. M. Steinberg, Amplifying Single-Photon Nonlinearity Using Weak Measurements, *Phys. Rev. Lett.* **107**, 133603 (2011).
- [39] Y. Kedem, Using technical noise to increase the signal-to-noise ratio of measurements via imaginary weak values, *Phys. Rev. A* **85**, 060102(R) (2012).
- [40] A. N. Jordan, J. Martínez-Rincón, and J. C. Howell, Technical Advantages for Weak-Value Amplification: When Less Is More, *Phys. Rev. X* **4**, 011031 (2014).
- [41] J. Harris, R. W. Boyd, and J. S. Lundeen, Weak Value Amplification Can Outperform Conventional Measurement in the Presence of Detector Saturation, *Phys. Rev. Lett.* **118**, 070802 (2017).
- [42] A. Nishizawa, K. Nakamura, and M.-K. Fujimoto, Weak-value amplification in a shot-noise-limited interferometer, *Phys. Rev. A* **85**, 062108 (2012).
- [43] D. Li, T. Guan, Y. He, F. Liu, A. Yang, Q. He, Z. Shen, and M. Xin, A chiral sensor based on weak measurement for the determination of proline enantiomers in diverse measuring circumstances, *Biosens. Bioelectron.* **110**, 103 (2018).

- [44] X. Zhou, W. Cheng, S. Liu, J. Zhang, C. Yang, and Z. Luo, Tunable and high-sensitivity temperature-sensing method based on weak-value amplification of Goos-Hänchen shifts in a graphene-coated system, *Opt. Commun.* **483**, 126655 (2021).
- [45] T. Guan, Y. Yang, Q. Zhang, Y. He, N. Xu, D. Li, L. Shi, Y. Xu, and X. Wang, Label-free and non-destruction determination of single- and double-strand DNA based on quantum weak measurement, *Sci. Rep.* **9**, 1891 (2019).
- [46] X. Zhu and Y.-X. Zhang, Influence of environmental noise on the weak value amplification, *Quantum Inf. Process.* **15**, 3421 (2016).
- [47] J. Sinclair, M. Hallaji, A. M. Steinberg, J. Tollaksen, and A. N. Jordan, Weak-value amplification and optimal parameter estimation in the presence of correlated noise, *Phys. Rev. A* **96**, 052128 (2017).
- [48] Y. Lee, T. Cheatham, and J. Wiesner, Application of correlation analysis to the detection of periodic signals in noise, *Proc. IRE* **38**, 1165 (1950).
- [49] Y. Liu, J. Liu, and R. Kennel, Frequency measurement method of signals with low signal-to-noise-ratio using cross-correlation, *Machines* **9**, 123 (2021).
- [50] E. J. Takahashi, P. Lan, O. D. Mücke, Y. Nabekawa, and K. Midorikawa, Attosecond nonlinear optics using gigawatt-scale isolated attosecond pulses, *Nat. Commun.* **4**, 2691 (2013).
- [51] R. Jozsa, Complex weak values in quantum measurement, *Phys. Rev. A* **76**, 044103 (2007).
- [52] Y. Susa, Y. Shikano, and A. Hosoya, Optimal probe wave function of weak-value amplification, *Phys. Rev. A* **85**, 052110 (2012).
- [53] S. Qaisar, R. M. Bilal, W. Iqbal, M. Naureen, and S. Lee, Compressive sensing: From theory to applications, a survey, *J. Commun. Netw.* **15**, 443 (2013).
- [54] https://www.thorlabschina.cn/newgrouppage9.cfm?objectgroup_id=4047
- [55] C.-F. Li, X.-Y. Xu, J.-S. Tang, J.-S. Xu, and G.-C. Guo, Ultra-sensitive phase estimation with white light, *Phys. Rev. A* **83**, 044102 (2011).
- [56] S. Carrasco and M. Orszag, Weak-value amplification of photon-number operators in the optomechanical interaction, *Phys. Rev. A* **99**, 013801 (2019).
- [57] Y. Turek, W. Maimaiti, Y. Shikano, C.-P. Sun, and M. Al-Amri, Advantages of nonclassical pointer states in postselected weak measurements, *Phys. Rev. A* **92**, 022109 (2015).
- [58] J. Reedy and S. Lunzmann, *SAE 2010 Commercial Vehicle Engineering Congress* (SAE International, Washington, DC, 2010).